

REX Radiometer Calibration at 4.2 cm on New Horizons

I. R. Linscott^{a,*}, D. P. Hinson^{a,b}, G. L. Tyler^a, S. A. Stern^c, L. A. Young^c, R. A. Beyer^{b,d},
M. K. Bird^{e,f}, K. Ennico^d, G. R. Gladstone^g, C. B. Olkin^c, M. Pätzold^e, P. M. Schenk^h,
D. F. Strobelⁱ, M. E. Summers^j, H. A. Weaver^k, W. W. Woods^j, The New Horizons
ATM Theme Team, The New Horizons Science Team

^a*Department of Electrical Engineering, Stanford University, Stanford, CA 94305, USA*

^b*Carl Sagan Center, SETI Institute, Mountain View, CA 94043, USA*

^c*Southwest Research Institute, Boulder, CO 80302, USA*

^d*NASA Ames Research Center, Moffett Field, CA 94035, USA*

^e*Rheinisches Institut für Umweltforschung, Universität Köln, 50931 Cologne, Germany*

^f*Argelander Institut für Astronomie, Universität Bonn, 53121 Bonn, Germany*

^g*Southwest Research Institute, San Antonio, TX 78238, USA*

^h*Lunar and Planetary Institute, Houston, TX 77058, USA*

ⁱ*The Johns Hopkins University, Baltimore, MD 21218, USA*

^j*George Mason University, Fairfax, VA 22030, USA*

^k*The Johns Hopkins University Applied Physics Laboratory, Laurel, MD 20723, USA*

^j*Capella Space Systems, Palo Alto, CA 94303, USA*

Abstract

REX is the **R**adioscience **E**xperiment on-board New Horizons. One part of the REX investigation, referred to as REX radiometry, measures the total RF power in two polarizations at X-band for radio frequencies illuminating the spacecraft's 2.1 m high gain antenna (HGA). The conversion of REX samples to physical units of RF power and equivalent temperature incorporates a scaling procedure with coefficients that were determined during pre-launch Integration and Test, as well as the spacecraft's Commissioning after launch in April 2006, and an additional Calibration Campaign in July 2016. The REX Radiometer calibration involved measuring post-launch both extended and compact sources of known X-band RF power from astronomical and solar system targets. Measurements of these sources are used in a multi-dimensional optimization to obtain the constants to convert the REX Radiometric engineering units to physical units as well as establishing the noise temperature of the New Horizons spacecraft's X-band receiver.

1.0 Introduction

Radiometric measurement of total X-band power with REX, the **R**adioscience **E**xperiment on-board New Horizons, is performed using the spacecraft's high gain antenna (HGA) with right-hand circular and left-hand circular polarization feeds, the spacecraft's two X-band receivers, with dedicated radiometric channels for each polarization, and dual REX processors. REX digitizes at Nyquist sample rates and computes the total RF power in each of the two polarization channels of the spacecraft's X-band receiver. A detailed description of REX and the Radioscience experiments on the New Horizons Mission is found in [Tyler, et. al., 2008].

The total RF power in REX digitized units is converted to RF power in physical units, such as dBm and an equivalent temperature in Kelvin (K), using conversion constants, or coefficients, that were determined in four calibrations performed over the course of the mission. A review of the New Horizons Mission to Pluto, and the presentation of the first results is in [Stern, et. al., 2015]. The first calibration performed before launch measured the HGA's response and the receiver noise temperature without the HGA. The second calibration was performed during the Commissioning of the New Horizons Spacecraft after launch during April and June 2006. A third calibration measurement was made during the Pluto Encounter due to a serendipitous scan across the sun. A fourth, post-Pluto encounter calibration was performed during a dedicated Calibration Campaign, in July 2016. During these calibrations REX measured (a) X-band receiver stability, (b) X-band receiver linearity, (c) the High Gain Antenna (HGA) response, (d) radio sky background, (e) X-band power from standard radio sources, and (f) total power from the Sun.

Calibrating the conversion of REX measurement to physical quantities with a precision of order 10%, involves 1% measurements of at least two X-band radio flux standards. However, the radiometric measurement objectives of the New Horizons Mission imposed requirements of at least 1% radiometric precision [Tyler, et.al., 2008]. To achieve this precision, a much larger suite of radio flux standards was incorporated along with a variety of methods of determining the calibration coefficients. What follows in this paper is a presentation of these methods, often with inconsistent results, and an approach for reconciliation to obtain a self-consistent, statistically significant and algorithmically stable solution for the REX radiometric conversion constants.

In this paper, Section 1.1 describes the overall measurement objectives, and Section 2 presents the calibration procedure. Section 2.0 discusses the radiometric characteristics of the X-band receiver, Section 2.1 the X-band receiver stability determination, Section 2.2 the X-band receiver linearity, and Section 2.3 the HGA response. Section 3.0 discusses calibration using known radio sources, and Section 4.0 provides an example of the conversion procedure using the calibration constants.

1.1 Radiometric Calibration Measurement Objectives

REX quantifies the total RF power in the 4.5 MHz radiometric channel of the New horizons X-band Receiver, in both right-hand circular polarization (RCP), and left-hand circular polarization (LCP). A detailed description of the New Horizons X-band Receiver and Telecommunications System is in [Deboy, et. al., 2007] and the Telecommunications interface to REX is described in [Deboy, and Funk, 2003].

The two radiometric channel polarizations are quantified by sampling the RCP and LCP RF voltages to a precision of 16-bits, at a rate of 10 Msamples/sec. The REX processor computes and integrates total RF power by squaring the voltage samples and accumulating the squared values in a 40-bit register. The register is cleared once every 1.024 seconds, and the register's value is output by REX ten times in the 1.024 second interval into the REX high-speed data stream. The REX data in each of the 1.024 second intervals is packaged into a data segment called a REX frame. Each REX frame is formatted and retrieved from the New Horizons spacecraft and archived in the New Horizons Science Operations Center (SOC), as a file with a unique name labeled by the Mission Elapsed Time or MET.

An idiosyncrasy of the REX process is the largest and last value in the power accumulator register is placed in the REX output as the first sample of the radiometer in the following REX frame. The operational procedures developed for the New Horizons Mission and the Pluto Encounter are discussed in [Sepan, et.al., 2016].

The 40-bit samples of the total RF power in the REX radiometric channels are a representation of the total RF power produced by the spacecraft's X-band receiver. This RF power is the sum of the RF power illuminating the spacecraft's High Gain Antenna (HGA) in the 4.5 MHz radiometrics band centered at 7.18 GHz, and the RF noise power from the X-band receiver itself. The REX 40-bit radiometric samples are in what are called REX units, and the RF noise power from the X-band receiver is typically identified as the receiver's noise temperature in units of Kelvin.

The primary objective of the REX radiometric calibration is to determine in each of the polarizations the value of the scaling constant that converts REX units to degrees kelvins, and to measure the noise temperature of the receiver. In principle, two sufficiently independent measurements in each polarization would be necessary to determine the two unknowns. However, the measurements can be perturbed by unknown factors that result in systematic errors. To protect against potential systematic effects, measurements were made of more than the minimum necessary sources. This leads to what is typically called an over-constrained condition, necessitating an optimization for the determination of the unknowns.

The calibration objective of the REX radiometer was thus performed as an over-constrained optimization for the two unknowns, (1) the REX units to kelvin conversion constants, and (2) the X-band receiver's noise temperature. A total of ten (10) sources of known radio power or temperature were observed with REX over the course of the New Horizons Mission. These radio sources are in three general classes: (a) weak, compact objects, essentially point astronomical sources with known radio flux, (b) weak, diffuse objects on the sky with a temperature at or near the temperature of the cosmic microwave background (called cold sky), and (c) strong, non-compact objects with known X-band noise temperature. A summary of these radio sources is listed in Table 2.0.1. The source strengths for the objects listed in Table 2.0.1, were taken from (a) the HEASARC Archive, (b) Perley et.al., 1984, (c) Rebold et.al., 1988, and (d) Vinyaikin, 2014.

In principle, any pair of REX radiometric observations in the set of known radio power would allow for the retrieval of the two calibration unknowns. But not every pair is sufficiently independent to produce results that are of useful precision or free of systematic errors. For example, any two of the cold sky observations are nearly identical and provide no useful constraint on determining the unknowns. For this reason it was important to include members of all three observational classes in an over-constrained optimization.

Name	Origin	Illumination	Strength	Type	Position (J2000)
Taurus-A ^(a)	Astronomical	Compact	578 jy	weak	RA 05:34:32 dec +22:00:53
Cass-A ^(a)	Astronomical	Compact	459 jy	weak	RA 23:23:24 dec +58:48:54
Cygnus-A ^(a)	Astronomical	Compact	231 jy	weak	RA 19:59:33 dec +40:43:41
Virgo-A ^(a)	Astronomical	Compact	53 jy	weak	RA 12:30:49 dec +12:23:28
Cold SkyA ^(b)	Microwave Background	Diffuse	2.7 K	weak	RA 06:04:48 dec +17:54:00
Cold SkyB ^(b)	Microwave Background	Diffuse	2.9 K	weak	RA 05:54:28 dec +13:24:00
Cold Sky C ^(b)	Microwave Background	Diffuse	3.1 K	weak	RA 06:15:12 dec +13:24:00
The Sun ^(d)	Solar System Object	Compact	1759 jy	medium	RA 07:00:18 dec +20:47:36
Galactic Center ^(a)	Astronomical	Diffuse	40 K	medium	RA 17:45:40 dec -29:00:28
Jupiter Equatorial ^(c)	Solar System Object	Diffuse	210 K	strong	RA 16:45:00 dec +17:00:00
Jupiter Polar ^(c)	Solar System Object	Diffuse	210K	strong	RA 03:15:00 dec +17:00:00

Table 2.0.1. Radio Sources with Known Power Used in the REX Radiometer Calibration. The superscripts in parenthesis are the references listed in text above this table.

2. Radiometric Characteristics of the REX Receivers

Radiometric measurement of equivalent temperature is based on the assumption the radiometric power from a target is thermal in its nature, i.e. radiated from a black-body process such that samples of radiometric power are from a Gaussian statistical distribution and statistically independent when sampled at intervals in time τ , equal to the reciprocal of the sampling bandwidth, B . i.e. $\tau \geq 1/B$. Under this assumption, the statistical precision of the radiometric power, σ , can be improved by integrating, or averaging, the samples, with the improvement scaling by the square-root of the number of samples. i.e. $\sigma = \sigma_o/\sqrt{N}$. Ideally, this improvement is unbounded, i.e. N can be arbitrarily large. However, the stability of the receiver's gain, and the linearity of the receiver's amplifiers effect an upper bound on N , or equivalently, the integration interval. Further, the $1/\sqrt{N}$ scaling of the standard deviation (STD), of the samples of power is limited if the statistical nature of the samples of radiometric power is not Gaussian.

The calibration of the REX radiometer has therefore a preamble to establish the extent of the receiver's stability, its linearity, and the statistical nature of the distribution of its radiometric power samples. These three characteristics are evaluated and discussed in Section 2.1 for stability and the nature of the statistical distribution, and Section 2.2 for linearity.

2.1 X-band Receiver Stability

The statistical lower bound for the precision of a REX thermal measurement, with an integration time of one second, is 0.068 K. This derives from the REX 4.5 MHz bandwidth Radiometrics Channel, (with greater than Nyquist sampling of 10 Msamples/sec), and the 146 K, noise temperature of the New Horizon X-band receiver (see Section 3, for the discussion of the receivers' noise temperatures). To realize this lower bound, the gain of the receiver must be stable enough that the effective noise temperature variations of the receiver are significantly smaller than 0.068 K on a time scale of ≥ 1 seconds.

In order to assess the receiver's stability, the gain variability was measured regularly, on a cadence of at least once per year, during New Horizons' cruise to Pluto. For these measurements, the HGA was pointed to a position on the sky with the lowest X-band brightness temperature. This location, called 'Cold Sky', with coordinates RA 15.2 degrees, and DEC, -8.1 degrees, and an X-band brightness temperature of 2.8 K, very near the lower limit afforded by the Cosmic Microwave Background, and over an angular size ten times larger than the 3 dB angular diameter of the HGA (i.e. 1.2°). The spacecraft pointing was controlled within a deadband of 0.1° , when REX acquired radiometric data. In assessing gain stability, the REX data acquisition duration was typically 1000 seconds.

The stability of the X-band receiver's radiometrics channel is evaluated from the fluctuation distributions of the REX Cold Sky radiometer data. The shape of the distribution as well as the mean and standard deviation (STD or σ), is computed for dyadically scaled integration times from a single sample to a few 100 seconds.

The variation of REX radiometric power and its fluctuation distribution are illustrated with the set of figures 2.1.1 to 2.1.3. REX computes the square magnitude of Nyquist sampled RF voltages in the X-band receiver's Radiometrics channel. These samples are digitized at 10 Msamples/sec, and accumulated in REX on a 0.1024 sec cadence. The accumulated sum is recorded 10 times per REX frame. The REX frame rate is one frame every 1.024 seconds. As an example, the first ~200 radiometer samples on the 0.1024 second cadence integration are shown in Figure 2.1.1.a, (RCP channel), and Figure 2.1.1.b, (LCP channel).

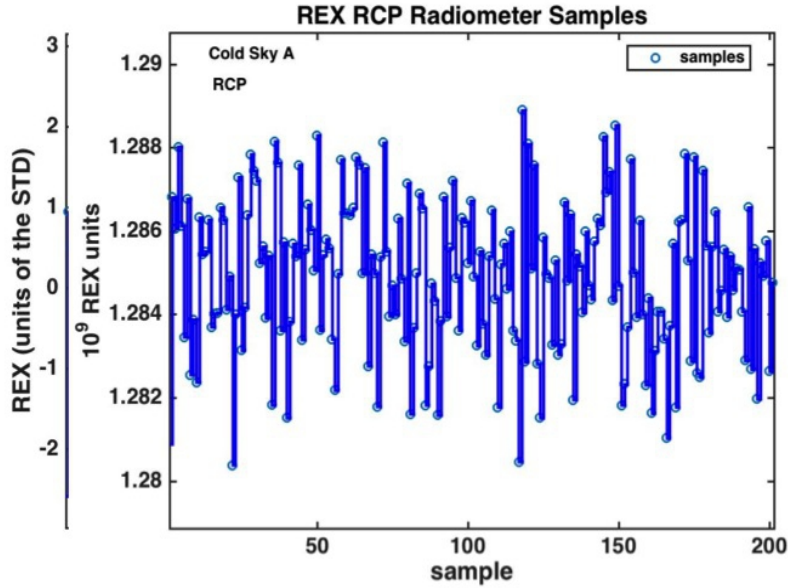


Figure 2.1.1.a. Samples of total power from the source Cold Sky A, for REX radiometric channel A, (RCP) on 11 July 2016. HGA pointing to Cold Sky. The total power is in 10^9 REX engineering units. The samples are at a rate of 0.1024 samples/sec. An additional scale has been added in units of the standard deviation (STD) of the total power samples. One STD is 0.002×10^9 REX units, or 1/642 of the mean total power.

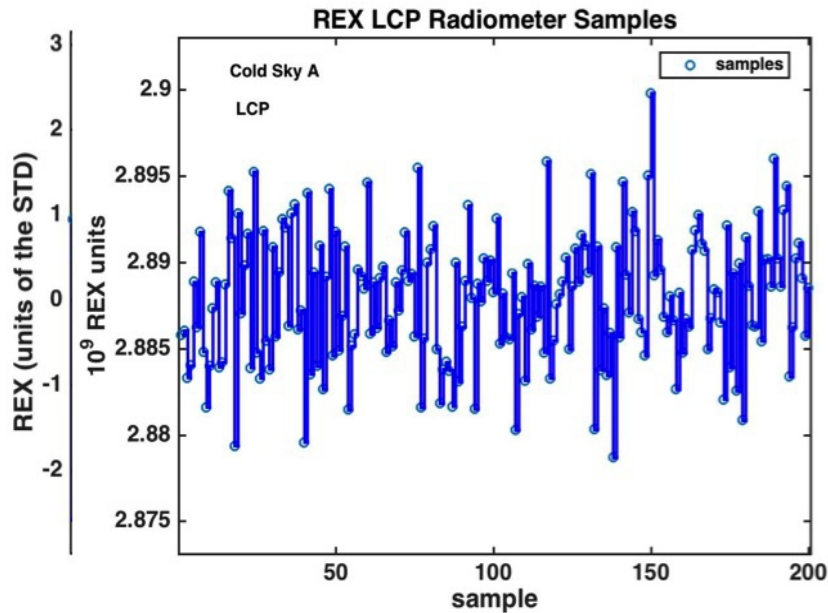


Figure 2.1.1.b. Samples of total power from the source cold Sky A for REX radiometric channel B, (LCP) on 11 July 2016. HGA pointing to Cold Sky. The total power is in 10^9 REX engineering units. The samples are at a rate of one sample per 0.1024. An additional scale has been added in units of the standard deviation (STD) of the total power samples. One STD is 0.005×10^9 REX units, or 1/578 of the mean total power. Note, the gain of the LCP channel is approximately twice that of the RCP channel.

The samples are displayed in “REX units”, and scaled by their standard deviation (STD). The samples appear to be random samples from an apparent Gaussian distribution with a mean of $\sim 1.285 \times 10^9$, for RCP, and $\sim 2.885 \times 10^9$, for LCP, and their widths equal to the STD's of a Gaussian. The approximately 2x difference of the mean power between RCP and LCP is due to a higher gain setting of LCP relative to RCP.

The REX samples are expected to form a normal distribution if the RF power sampled by REX is from the illumination on the HGA of thermal radiation with a black-body spectrum. Further the RF power distribution's STD should scale with the equivalent black-body temperature of the source of the thermal radiation. Thus, the shape of the distribution of REX samples of total power in the radiometrics channels should reveal if the combined radiation from Cold Sky and noise from the X-band receiver are consistent as having come from a thermal process with a black-body spectrum. By way of confirmation, the distribution of REX total RF power, formed from samples such as in Figures 2.1.1a, and 2.1.1b, is presented in Figure 2.1.2, for both the RHC and the LHC polarization channels. A best-fit Gaussian is overlaid in each of the plots. The statistical confidence, a chi-squared value, is added in red font. The chi-square is the mean of the fit's squared residuals weighted by the statistical uncertainty of the population of each histogram bin.

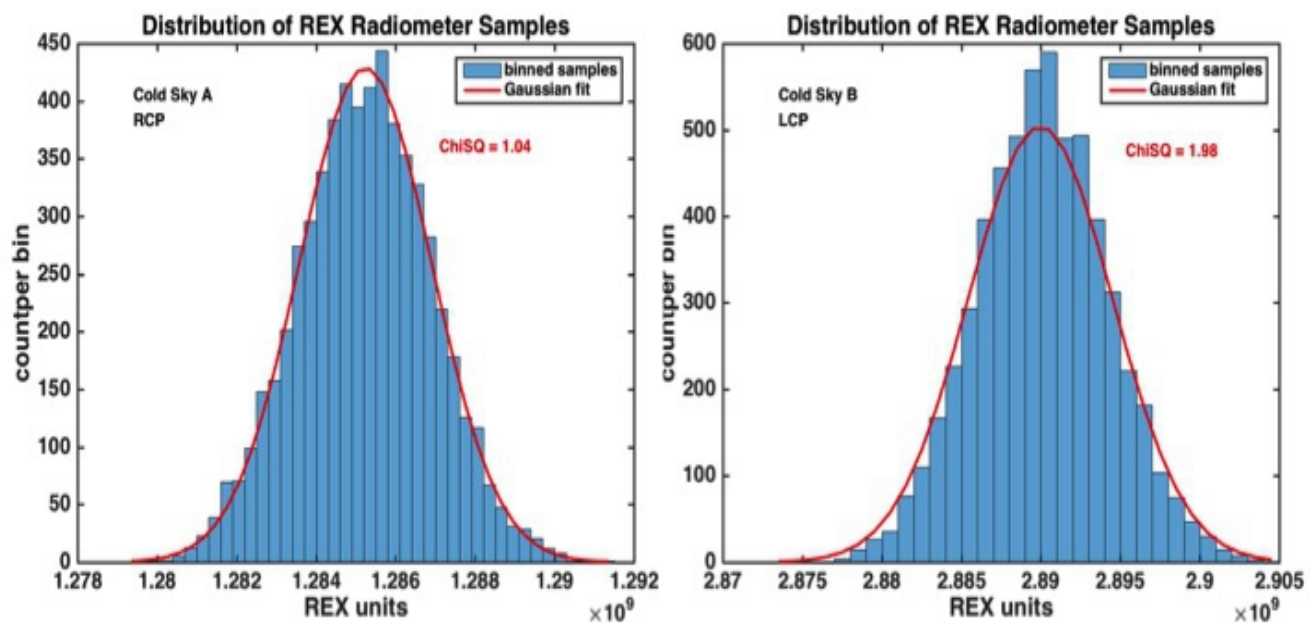


Figure 2.1.2. Distribution of the REX samples of total power with Gaussian fits in the X-band receiver's radiometric channels. The data is from an extended REX acquisition of 1000 seconds, taken on August 2016. The left side plot is for RCP, and the right side plot is LCP.

This chi-square is 1.04, and 1.98, for the RHC and LHC channels in Figure 2.1.2, respectively, confirming the assumption of a thermal, black-body process. The Gaussian fits were performed as a three-dimensional optimization of the distribution's mean, STD and amplitude. The mean value of the REX samples is a statistically stable, robust measure of the noise power, and the ratio of the STD to the mean should scale according to the $1/(\text{square-root})$ of the number of samples averaged to compute the mean.

The extent of the scaling of the STD with (no. of samples)^{-0.5} tests the additional assumption that the REX radiometric samples are statistically independent. For instance, if the X-band receiver's gain is not constant, but varies perhaps slowly and by a small amount over the intervals used for averaging, then the REX samples will not be strictly independent, but possess a correlation on the time scale of the gain variation. This correlation adversely impacts the 1/(square-root) scaling.

To evaluate the scaling the standard deviation of the mean, the REX radiometer samples from cold sky targets are averaged over contiguous blocks of time. The standard deviations, σ_{STD} , are computed from the set of block averages of radiometer power. The REX samples are segmented into M sets of equal time intervals $N_M \tau_a$, where $\tau_a = 0.1024$ sec, and N_M , is the number of samples in the interval. The mean power is computed in each interval and the standard deviation of the means is computed over the set M. The length of the time interval is increased by a factor of two, and the process is repeated, for as long as the number of intervals M, is large enough to be statistically significant (i.e. $M \geq 4$). The scaling of σ_{STD} with N_M , for the Cold Sky data is shown in Figure 2.1.3.

From the behavior seen in Figure 2.1.3, REX's radiometer σ_{STD} , decreases with increasing integration time as $1/\sqrt{N_M}$ for integrations up to ~ 100 samples. For longer integrations, the decrease is at a slower rate. The change at an integration of ~ 100 samples, indicates there is a transition from statistical independence to partial interdependence, i.e. the onset of sample to sample correlation, likely the consequence of gain variation in the receiver. Even so, the gain of the New Horizons X-band receiver is sufficiently stable for integrating radiometer power for time intervals of up to 100 sec to a precision of $0.068 \text{ K}/\sqrt{N_M}$. At the sample rate of 10 Msamples/sec, and an integration time of 100 seconds, the statistical decrease in the STD of the power is $1/\sqrt{10^9}$ samples, or 0.33×10^{-4} for a 100-s integration. Importantly, the REX radiometrics channel bandwidths are 4.5 MHz, and at 10 Msamples/s, the samples are not sample-to-sample statistically independent. The decrease in STD with integration is then expected to be $1/\sqrt{4.5 \times 10^8}$, or 0.47×10^{-4} . At a noise temperature 146 K, for the X-band receiver, the resultant precision of a REX radiometer power measurement is 0.0068 K, for a 100-s integration.

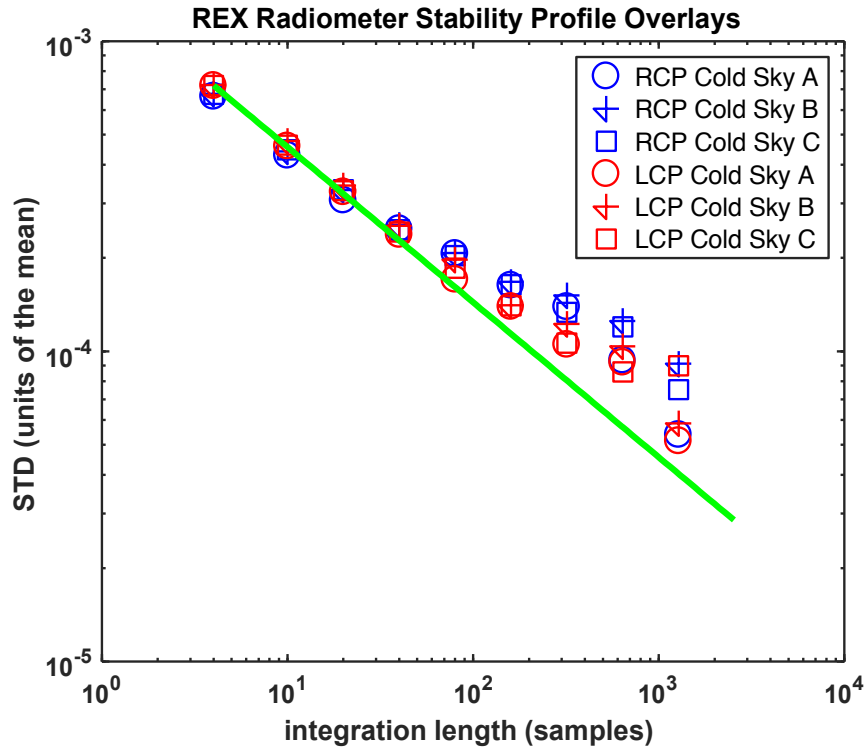


Figure 2.1.3. The standard deviation (STD) of REX total power samples. For this profile the radiometer sample rate of 10 samples per 1.024 seconds was used. The STD was evaluated over a range from four samples to 1280 samples. Profiles are shown for three cold sky locations and two polarizations each. The green dotted line has a slope of $1/\sqrt{N_M}$.

2.2. X-band Receiver Linearity

In addition to stability, it is highly desirable that the radiometer power produced by REX is a linear response to the RF power illuminating the receiver's antenna. To verify this was the case, the end-to-end response of the X-band receiver was measured post-launch during spacecraft commissioning, and at every annual checkout. The gain of the receiver was stepped in intervals of twice the minimum gain change, or 2×0.475 dB, while REX recorded radiometer power and narrowband waveforms of high power uplink transmission from earth. Uplink CW signal were transmitted by NASA's Deep Space Network (DSN) antennas, radiating up to 20 kWatts from 34-m and 70-m antennas. A description of the DSN operation and protocols may be found in Sepan, et.al., [2016]. The uplink radiated power was adjusted to produce an RF illuminating power on the spacecraft of a nominal -112 dBm. This illumination increased the REX radiometric channel power by $\sim 10\%$, and produced a narrow-band signal in the REX band with an SNR of ~ 55 dB/Hz. These measurements have a precision of ~ 0.025 dB for each gain step of ~ 1 dB, thereby providing the capability to assess the end-to-end linearity of the power measurement from earth transmission to REX data samples.

An example of the REX radiometer power profile obtained while the gain was stepped in ~ 1 dB increments is shown in Figure 2.2.1. The 'staircase' of expected power change is consistent with the measured change, confirming the linearity of the REX power with the selected gain. Typically, the

uplink power varies by ~ 0.25 dBm within each of the gain steps. This is attributed to the variation in the uplink power due to small variations in transmitted power at the source as well as dead-band pointing variations and propagation effects along the ~ 30 AU radio path from earth to the spacecraft. For Figure 2.2.1, these variations have been removed, leaving only statistical fluctuations, to improve verification of linearity and a comparison between polarizations.

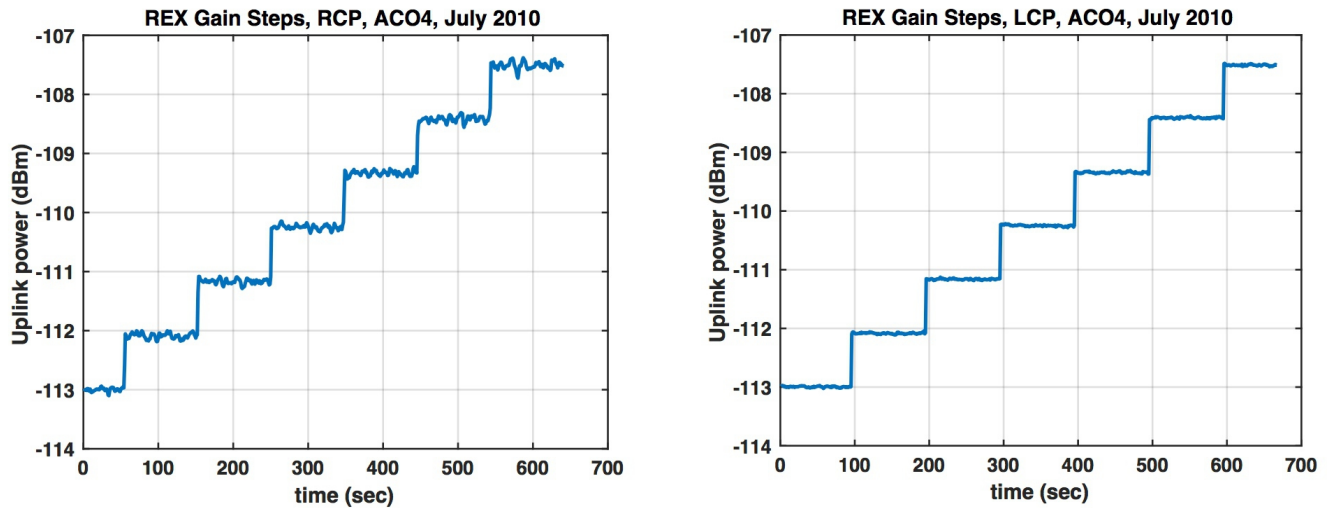


Figure 2.2.1. Steps in the received X-band power, during the 4th annual checkout of the spacecraft, i.e. ACO-4, in July 2010. The spacecraft's HGA was pointed to Earth, and nominal uplinks were transmitted to the spacecraft, one uplink in each polarization. During the 700 seconds of REX acquisition, the X-band receiver's gain was increased by equal steps in dB. The gain steps here are twice the X-band receiver's minimum gain adjustment. The minimum gain step was designed to be 0.475 dB/step. The gain steps in this figure vary slightly from the design amount, where the average over the six steps is 0.933 dB/step, or for an average of the minimum step of 0.466 ± 0.007 dB/step. The error is consistent with the design value, and 0.007 dB/step, is 0.16%. The uplink power has been compensated for variations due to spacecraft rotation and attitude control, as well as variations attributable to the radio path.

2.3 High Gain Antenna (HGA) response

The response of the High Gain Antenna's (HGA) to far-field RF illumination was measured before launch. These measurements were used to produce a 2D response and gain profile. During the post-launch spacecraft commissioning, the HGA response was re-measured by raster scanning the spacecraft's HGA across the direction to earth while an uplink transmitted from the DSN was acquired by REX. For this acquisition, the X-band signal in the REX band was downconverted to baseband and REX resolved the uplink power to a frequency resolution of 1 Hz. The SNR at this resolution was ~ 60 dB, suitable for resolving the HGA's sidelobes. Figure 2.3.1, shows the HGA's response obtained from pre-launch measurements [Schulze, 2017]. Figure 2.3.2, and 2.3.3, show the HGA's post-launch measurements for both REX radiometric channels.

Pre-Launch HGA Response

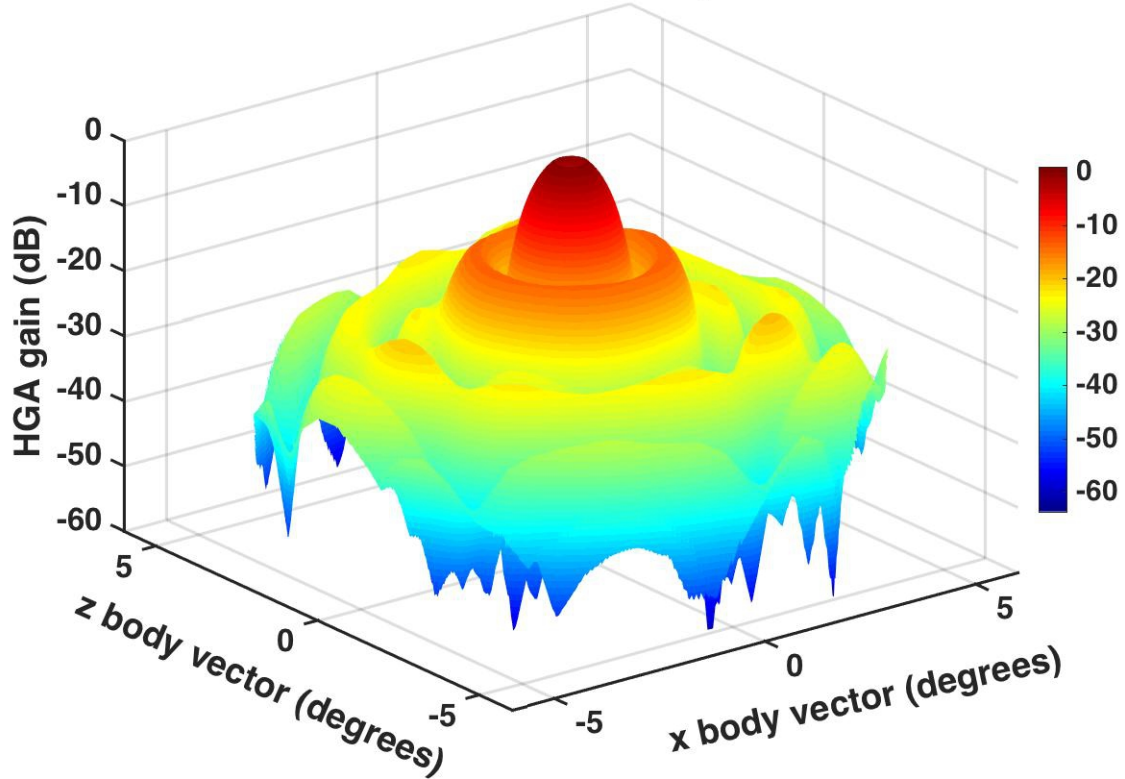


Figure 2.3.1 Pre-launch response of the HGA out to 5° elongation from the boresight. See [Schulze, 2015], for a discussion of the measurement process.

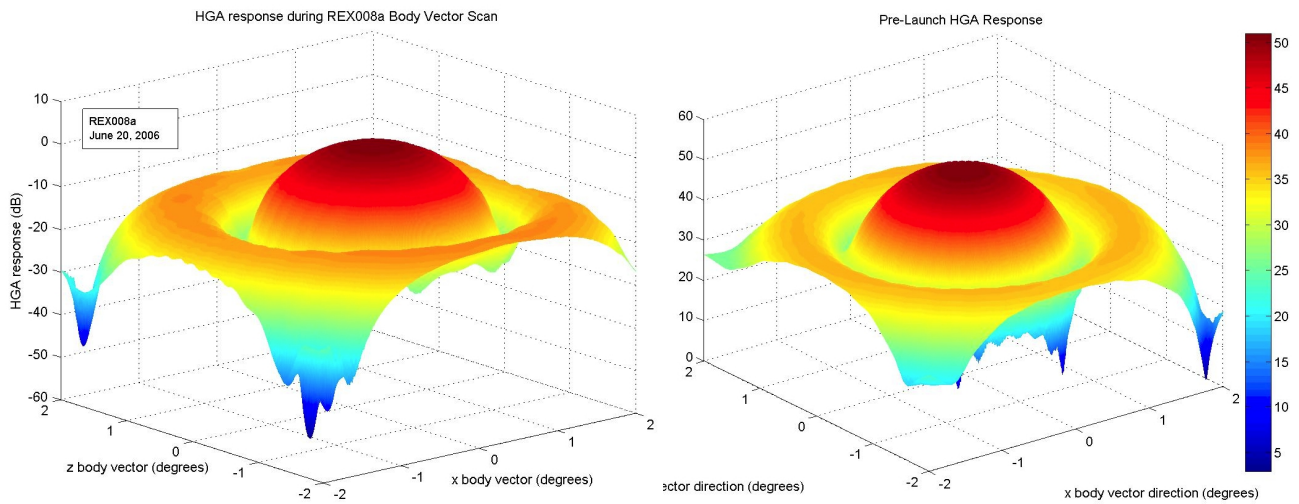


Figure 2.3.2. Left hand figure is the HGA's response in REX measured during spacecraft commissioning, 2006. Right hand figure is the HGA's response as measured before launch. The gain relative to boresight is shown for elongation angles less than 2°.

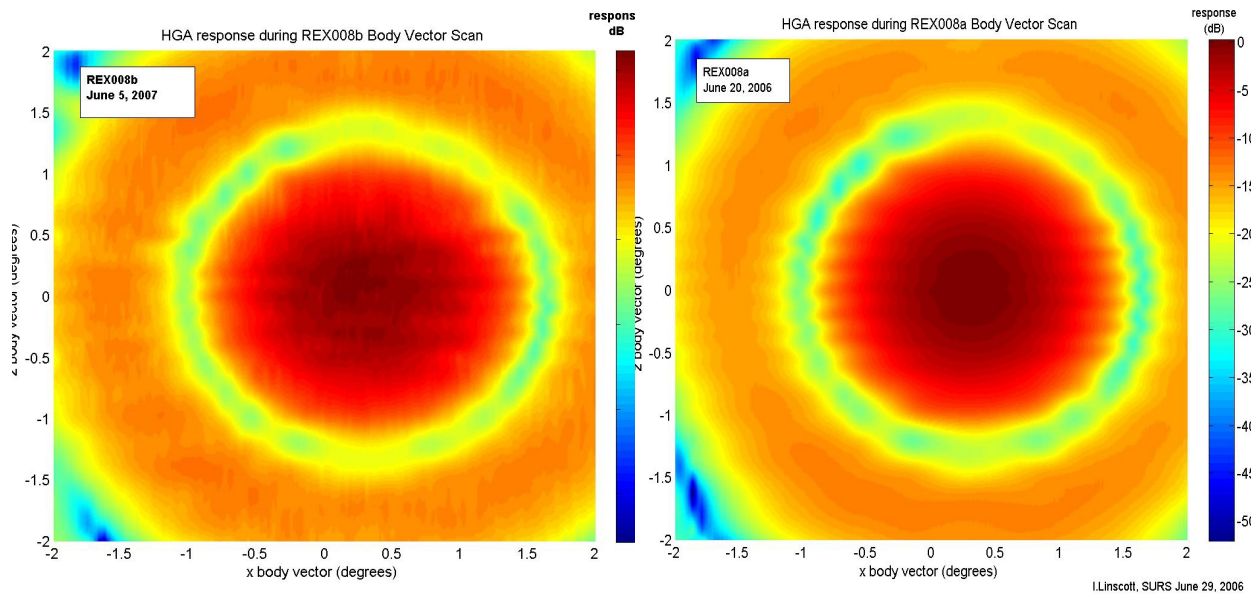


Figure 2.3.3. HGA response as measured by scanning the HGA across an uplink. Left hand figure is HGA response for Left Hand Circular polarization (LCP), and the right hand plot is the HGA's response for Right Hand circular polarization (RCP)

3.0 Calibration of REX using Known Sources of Radiometric Power

REX produces samples of the RF power in the New Horizons X-band Receiver's Radiometrics Channel, a heterodyned representation of the radio frequencies in a 4.5 MHz band centered at 7.18 GHz. The REX power values are in “REX Units”, unscaled 40-bit representations of the squared-and-accumulated digitized samples from the Radiometrics Channel. The conversion of REX units to physical units such as temperature in degrees Kelvin, or RF power in watts (or more often, dB relative to a milliwatt - dBm), is a linear scaling using a single conversion constant and knowledge of the receiver's noise figure (or noise temperature) for both RCP and LCP.

3.1 Radio Sources for Calibration

The relationship between a source of thermal electromagnetic radiation and the radiometric power received by New Horizons' High Gain Antenna (HGA), and X-band receiver can be distilled to just a few parameters. First there is the thermal source itself, and the proportionality expressed by Boltzmann's constant, $k_{Boltzmann}$, between equivalent temperature and radiometric power, if the source is indeed *thermal*, possessing a frequency spectrum of black-body radiation. Then only a few parameters relate the radio-frequency power from the radio source, and perhaps the background sky, illuminating the HGA to the X-band receiver's conversion into detectable and quantifiable RF power presented to the REX Radiometer. Added to this is the noise power intrinsic to the receiver itself. The parameterization the relationship between thermal source temperature and radiometric power is stated in Eqn. 3.1.1.

$$RU_{Src, Pol} = G_{REXtoK_{Pol}} \left(\frac{1}{2} \eta T_{Src} + \frac{1}{2} (1 - \eta) T_{sky} + T_{RX_{Pol}} \right) \quad (3.1.1)$$

Boltzmann's constant has been incorporated into $G_{REXtoK_{Pol}}$, and the subscript Src , denotes the thermal source, and Pol , is the polarization, either Right-Hand Circular (RHC), or Left-Hand Circular (LHC). Several scenarios are included in Eqn. 3.1.1, accommodated by the solid angle fraction η . For instance, if the thermal source is spatially diffuse and extends well beyond the angular size of the HGA's response (or 'beam'), then $\eta = 1$, and no background power enters the HGA, (i.e. $T_{sky} = 0$). Specifically, if the HGA is pointed to the radiometric coldest part of the sky then $\eta = 0$, and $T_{sky} = 2.7$ K. A third scenario is when the thermal source is a point source of known radiometric flux. Then η is essentially zero, but the T_{Src} term remains in the form of an integral of the source's flux over the HGA's illumination aperture. The HGA's peak gain, determined from pre-launch tests, was 41.8 ± 0.2 dBi [R. Schulze, priv. comm.] This value for the gain gives an effective HGA area of, $A_{HGA} = 2.098$ m² and an aperture efficiency e_{HGA} , of 0.61. Eqn. 3.1.2, is the appropriate relationship for this case.

$$RU'_{Src, Pol} = G_{REXtoK_{Pol}} \left(\frac{1}{2k_{Boltzman}} \left(S_{Src, jy} e_{HGA} \pi \frac{D_{HGA}^2}{4} \right) + \frac{T_{Sky_{Src}}}{2} + T_{RX_{Pol}} \right) \quad (3.1.2)$$

However, for purposes of comparison, Eqn. 3.1.2, is cast in the form of Eqn. 3.1.1, as,

$$RU_{Src, Pol} = G_{REXtoK_{Pol}} \left(\frac{1}{2} T_{point_{Src}} + \frac{1}{2} T'_{sky} + T_{RX_{Pol}} \right) \quad (3.1.3)$$

In Eqns 3.1.1 to 3.1.3, $G_{REXtoK_{Pol}}$, is the conversion constant from REX units to Kelvin, and $T_{RX_{Pol}}$, is the X-band receiver's noise temperature, for polarization Pol . The factor of $\frac{1}{2}$, accounts for the apportionment of a presumed unpolarized source into two polarizations of equal gain. The sky temperature in Eqn. 3.1.3, is primed to indicate the point source is imbedded in the background sky, and the sky temperature is assessed as the integral of the sky distribution's temperature over the HGA's gain, exclusive of the point source's contribution.

Both $G_{REXtoK_{Pol}}$, and $T_{RX_{Pol}}$, are presumed unknowns and measurement of at least two fully HGA illuminating sources are needed for their determination. Unfortunately the only such sources for New Horizons, during its mission have been cold sky, i.e. portions of the sky at or near the temperature of the cosmic microwave background (CMB). Multiple radiometer measurements of cold sky while useful for validating long term stability of the receiver's gain, are degenerate for the purpose of determining the unknown parameters in Eqns. 3.1.1 to 3.1.3. In fact, the measurements of Cold Sky A,B,C were made twice, July 15, 2015 and July 11, 2016. A small difference in the value of RU was observed between these two dates.

X-band radiometric power is well known for many astronomical sources, a few of which observed with the HGA are comparable to the CMB and unfortunately marginally useful for resolving the degeneracy with the CMB measurements and Eqn. 3.1.1. The limiting factor is the 2.1m diameter of the HGA. Since 1 jy is 10^{-26} watts/m²/Hz, the equivalent temperature at the HGA, using Boltzmann's constant, is $1 \text{ jy} \times \pi(2.1/2)^2/k_{\text{Boltzmann}} = 7.59 \times 10^{-4}$ Kelvin. A 500 jy source is thus only comparable to the CMB's temperature, and a 5000 jy source would be needed for removing degeneracy in the CMB measurements. However there are no 5000 jy astronomical sources at New Horizons' X-band frequency. There are only a few in the range of 10 jy to 100 jy. The astronomical sources observed for the REX radiometer calibration are listed in Table 2.0.1. the strongest, Taurus-A, at 578 jy, yields only 0.44 K for each of the REX polarization channels.

Nevertheless, astronomical point sources do serve a useful purpose as an independent means to both estimate the HGA's efficiency and validate the calibration constants.

3.2 Finding an Optimum Set of Calibration Parameters

The sets of common unknown parameters in Eqn's 3.1.1, and 3.1.3, are the conversion constant $\text{GREX}_{\text{toK}_{\text{pol}}}$, and receiver noise temperature TRX_{pol} . These equations are almost in the form:

$$y_n = A_n x_1 + B_n x_2$$

where x_1 is the conversion constant and x_2 is the receiver noise temperature. Unfortunately when the conversion constant is multiplied through Eqns 3.1.1, and 3.1.2, x_2 contains x_1 , and the equations are no longer linear. But if they were, then the ensemble $\{RU_{mP}, RU'_{mP}\}$, could be represented by the matrix operator,

$$Y = A X$$

With Y a vector of the REX units, and X a vector of the unknowns, and A the matrix of known coefficients involving the source strengths. For vector size of the combined multiplicities N , of the calibration observations, the matrix A would be of size $N \times 2$, and using a singular value decomposition for A ,

$$A = U S V^*$$

Where S is square and diagonal, and U and V are the orthonormal basis SVD constructs. A least-squares optimum for the unknowns X , is obtained as,

$$X = [V S^{-1} U^*] A \tag{3.2.1}$$

A common means to linearize Eqns 3.1.1, and 3.1.3, in the unknown parameters, would be to adopt an iterative solution, where the product $x_1 x_2$, is $\text{GREX}_{\text{toK}_{\text{pol}}} \times \text{TRX}_{\text{pol}}$, and replaced by $G_e \text{TRX}_{\text{pol}}$, or $G_e x_2$ where G_e is a first estimate of $\text{GREX}_{\text{toK}_{\text{pol}}}$. Then Eqn. 3.2.1, is applied to obtain a least-squares solution for the 2×2 unknowns, and the estimate G_e , is updated and the process repeated if and until stable and converging values are found. A good measure for convergence is to use an L2 norm of the form.

$$\Omega = \sum_{n=1}^{N_d} w_{d,n} \left(R_{d,P} - RU_{n,P} \left(G_{\text{REXtoK}_P}, T_{\text{XB}_P} \right) \right)^2 + \sum_{n=1}^{N_C} w_{C,n} \left(R_{C,P} - RU'_{n,P} \left(G_{\text{REXtoK}_P}, T_{\text{XB}_P}, e_{\text{HGA}} \right) \right)^2 \quad (3.2.2)$$

and minimizing Ω , via a multi-dimensional search. The two parts of Eqn 3.2.2, are for the measurements of (i) the diffuse calibrators d , and (ii) the compact calibrators C . The measured quantities are $R_{d,P}$ and $R_{C,P}$ respectively, and the individual weights, $w_{d,n}$, and $w_{C,n}$, are given by the product of a class weight $e_{d,n}$, and $e_{C,n}$, that can emphasize (or deemphasize) any member of that class, and the one sigma value $\sigma_{d,n}$, and $\sigma_{C,n}$, of the measurement STD's.

$$w_{d,n} = e_{d,n} / \sigma_{d,n}$$

$$w_{C,n} = e_{C,n} / \sigma_{C,n} \quad (3.2.3)$$

An example of the character of Ω , over the 2D space of the conversion constant and receiver noise temperature, for each polarization is in Figure 3.2.1.

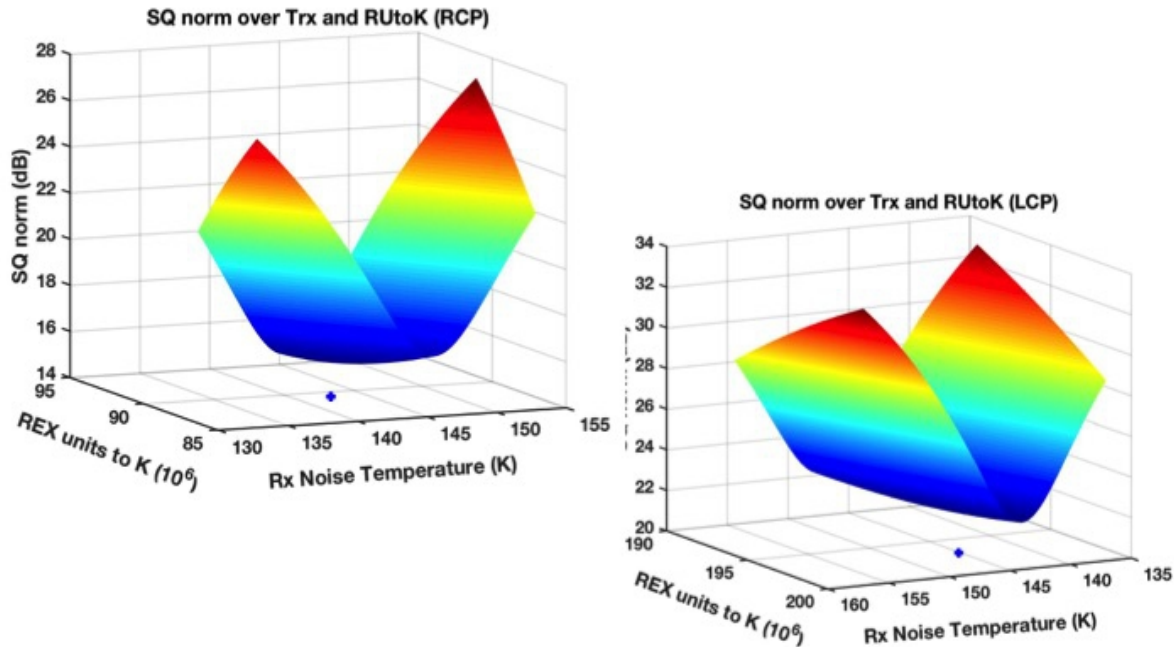


Figure 3.2.1. Optimization space of the Ω norm (i.e. L2 norm). Shown are the Ω surfaces over the 2D space spanned by the conversion constant $G_{\text{REXtoK}_{\text{Pol}}}$, and the receiver noise temperature TRX_{Pol} . The Ω surface for RCP is on the left and LCP is on the right.

The Ω surfaces in Fig. 3.2.1, were computed using measurements from the source list in Table 2.1.1. Details of these measurements are discussed in the later sections 3.3, for cold sky, 3.4, for radio astronomy standards, 3.5, for the sun, 3.6 for Jupiter, and 3.7, for earth transmissions.

An evident feature of the Ω surfaces in Fig. 3.2.1, is the shallow minimum contained in the valley formed by the wings of the Ω sheet. Although the long, narrow valley possesses a minimum point, as indicated by the location of the blue dots in Fig. 3.2.1, any point along the valley would be 'close' in terms of being a reasonably good choice for the optimum. The long narrow valley in shape of the Ω surface is not surprising given the near-degeneracy of the measurements.

The optimization search is performed in the three-dimensional space of G_{REXtoK_P} , T_{RX_P} , and e_{HGA} , the HGA efficiency. The HGA's aperture efficiency e_{HGA} , is included as a means to assess the possibility of a change in the response of the HGA after launch.

The three-dimensional optimization reaches a stable minima in the L2 norm after typically 100 to 200 iterations, with normalized values dominated by the measurement uncertainties. Notably, the optimization exhibited a strong sensitivity to just one of the measurements, the *Sun*. By deemphasizing the sun's measured value using the class weight, the optimization was stable, indicating the measured strength of the Sun possessed systematic uncertainties, likely due to the close proximity of the Sun to Pluto and the inability to be fully on-source, or fully off-source in the radiometric scan profile. The optimization produced the same stable results with values of the Sun's class weight less than 0.5. The class weights for all the other measurements was unity. Table 3.1.1, lists the optimized results for the three variables, using the measurement values listed in Table 2.0.1. The Jupiter scans were excluded from the optimization inputs.

Even though Jupiter was not used in the optimization, Jupiter was a much stronger source of thermal radiation in REX at the time of the two scans, and thus presents an opportunity to verify and validate the optimization values of conversion constants and receiver noise temperature. Unfortunately, at the time of the scans, less than a year after launch, the commissioning of the spacecraft had not completed certification of REX LCP data storage and access in the spacecraft's Solid State Recorder (SSR). Consequently, the Jupiter radiometric scans were done in RCP alone. However, the opportunity remains to use the Jupiter measurements to verify the RCP receiver noise temperature.

HGA RCP aperture efficiency	REX unit to Kelvin RCP	REX unit to Kelvin LCP	HGA LCP aperture efficiency	RCP Rx Noise Temperature	LCP Rx Noise Temperature
e_{HGA}	G_{REXtoK}	G_{REXtoK}	e_{HGA}	$T_{xb} (K)$	$T_{xb} (K)$
0.601 ± 0.001	$86.08 \cdot 10^6$ $\pm 0.1 \cdot 10^6$	$201.88 \cdot 10^6$ $\pm 0.1 \cdot 10^6$	0.602 ± 0.001	146.4 ± 0.1	144.4 ± 0.1

Table 3.1.1. Results from the three-dimensional optimization. The HGA aperture efficiency, the REX units to Kelvin conversion constant and the receiver's noise temperature were optimized to fit sources of known X-band thermal radiation listed in Table 2.0.1, with the exception of the Jupiter scans. The errors are statistical, arising from contributions from the ensemble of noise sources.

3.2.a Polarization Anomaly

The Thermscans are a pair of REX radiometric measurements of Pluto performed by scanning the HGA shortly after closest approach across chords of Pluto during the encounter. The coordinate system for the spacecraft was chosen such that the +Y axis was nominally in the direction of the HGA's boresight, the +Z axis was 'up' in the sense of the normal to the plane of the ecliptic, and the +X axis

was nominally 'horizontal' i.e. in the plane of the ecliptic. The first of the radiometric scans, in the +X direction, was along Pluto's diametric chord as seen from the spacecraft, and the second in the -X direction, back across the chord intersecting Pluto's winter pole. Applying the radiometric conversion using the calibration values in Table 3.1.1, gives radiometric brightness temperatures for the chords on Pluto, shown in Figure 3.2a.1.

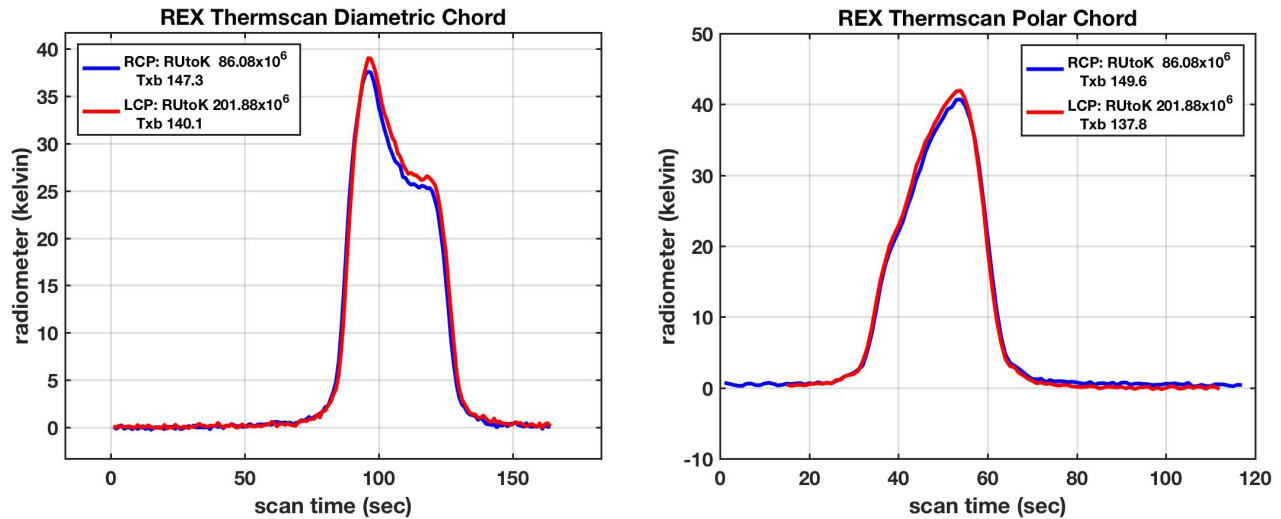


Figure 3.2a.1. Diametric and Polar Scans of Pluto. Plotted are the excess antenna temperatures over the background from the radiometric scans of Pluto, as seen from the spacecraft. Both RCP and LCP radiometric profiles are shown. The left side plot is the scan across the diametric chord. The right side plot is the radiometric scan of a chord that intersects Pluto's winter pole.

The angular diameter of the HGA footprint at Pluto was approximately one-eighth the angular diameter of Pluto during the scan. The edge of Pluto's disk occurs at the point where the temperature is one-half of its maximum, thereby defining the scan's chord across Pluto's surface. Several aspects of the temperature brightness profiles in Figure 3.2a.1, stand out as curiosities and even anomalies. First, the diametric and polar scans have distinct change in slope near where the scans cross the terminator. The antenna temperature is higher on the non-illuminated hemisphere. Secondly, the X-band receiver's noise temperature required a 0.1K adjustment in both polarizations to set the background excess temperature to zero, even though the temperature of the sky in the direction of the scans has been accurately estimated using published surveys. Third, the LCP profiles have a higher temperature over the chords than the RCP profiles. Significantly, the receiver's noise temperature corrections only increased the temperature difference between LCP and RCP profiles over the chords. This temperature difference appears in both the diametric and the polar profiles, suggesting Pluto's thermal radiation is slightly left-hand circularly polarized.

Linear polarization effects exist in radiometry, but a net circular polarization is very rare, especially for planetary bodies [Wielebinski, 2012]. To see if the other REX radiometer measurements in the calibration suite, (identified in Table 2.0.1), possessed the same anomaly, the REX radiometer units were converted to brightness temperature using the same conversion constants. Indeed, these profiles all exhibit the same polarization anomaly, where the LCP temperatures are slightly higher than the RCP temperatures. Notably, the REX units to temperature conversion constants were obtained as solutions

to a multi-dimensional optimization. They resided in a rather shallow minimum of the optimization metric, and within a narrow trough. Small perturbations of that solution away from the shallow minimum and along the trough would be comparably good in terms of the optimizations' metric. Perhaps a perturbation of the solution within the space of good solutions would give calibration constants and subsequent temperatures profiles that remove the polarization anomaly.

3.2.b Polarization Anomaly Resolution

If the radio sources listed in Table 2.0.1, are presumed unpolarized in circular polarization, the polarization labels can be removed from the source temperatures, and the conversion in Eqns. 3.1.1, 3.1.2, and 3.1.3, rewritten as Eqns. 3.2b.1, 3.2b.2, and 3.2b.3. Note, the receiver temperature, conversion constants and Rex units still retain their polarization labels, and T_{Src}^{max} denotes the maximum temperature measured during the HGA's scan across a source.

$$RU_{Src, Pol} = G_{REXtoK_{Pol}} \left(\frac{1}{2} \eta T_{Src} + \frac{1}{2} (1 - \eta) T_{sky} + T_{RX_{Pol}} \right) \quad (3.2b.1)$$

$$RU_{Src, Pol} = G_{REXtoK_{Pol}} \left(\frac{1}{2} T_{Src}^{max} + T_{RX_{Pol}} \right) \quad (3.2b.2)$$

$$RU_{Src, Pol} = G_{REXtoK_{Pol}} \left(\frac{1}{2} T_{sky} + T_{RX_{Pol}} \right) \quad (3.2b.3)$$

Here, Eqn 3.2b.2, is for the scan across a point source, and Eqn 3.2b.3, is for a measurement of an extended portion of cold sky. Two of these equations, Eqns. 3.2b.2, and 3.2b.3, are for sources that extend beyond the angular response of the HGA, and thus remove the angular response of the HGA from consideration. A minor rearrangement gives Eqns. 3.2b.4, and 3.2b.5.

$$\frac{RU_{Src, Pol}}{G_{REXtoK_{Pol}}} = \frac{1}{2} T_{Src}^{max} + T_{RX_{Pol}} \quad (3.2b.4)$$

$$\frac{RU_{Src, Pol}}{G_{REXtoK_{Pol}}} = \frac{1}{2} T_{sky} + T_{RX_{Pol}} \quad (3.2b.5)$$

Taking the difference in the same polarization between Eqns. 3.2b.4, and 3.2b.5, removes dependence on the receiver's noise temperature, as in Eqns. 3.2b.6. Defining the difference in REX units with Eqn. 3.2b.7, the result in Eqn. 3.2b.8, is independent of polarization as long as the assumption of an unpolarized source is correct.

$$\frac{1}{G_{REXtoK_{Pol}}} \left[RU_{Src, Pol}^{max} - RU_{sky, Pol} \right] = \frac{1}{2} \left(T_{Src}^{max} - T_{sky} \right) \quad (3.2b.6)$$

Defining the difference in the REX units as,

$$\Delta RU_{Src-sky,Pol} = RU_{Src,Pol}^{\max} - RU_{sky,Pol} \quad (3.2b.7)$$

and rewriting Eqn. 3.2b.6, as,

$$\frac{\Delta RU_{Src-sky,Pol}}{G_{REXtoK}_{Pol}} = \frac{1}{2} (T_{Src}^{\max} - T_{sky}) \quad (3.2b.8)$$

Shows the difference in REX units between source and sky, divided (or normalized) by the conversion constant, is polarization independent, under the assumption that the source and the sky are unpolarized. Equating Eqn. 3.2b.8, for RCP and LCP, produces the ratio in Eqn. 3.2b.9, that has been rearranged to relate the RCP conversion constant in terms of the LCP conversion constant. Importantly, Eqn. 3.2b.9, does not have any knowledge of the temperature or the flux strength of the source or the sky. Only the REX radiometers response in REX units is needed to obtain the ratio between the conversion constants, thereby allowing any of the REX radiometric measurements as a means of relating the calibration constant for the two polarizations.

$$G_{REXtoK}_{LCP} = G_{REXtoK}_{RCP} \frac{\Delta RU_{Src-sky,LCP}}{\Delta RU_{Src-sky,RCP}} \quad (3.2b.9)$$

An alternate formulation of Eqns. 3.2b.4 and 3.2b.5 similarly relates the receiver noise temperatures, again without knowledge of the strengths of the source and sky. For this purpose, take the difference again using Eqns. 3.2b.4, and 3.2b.5, but across the two polarization, as indicated in Eqns. 3.2b.10.

$$\begin{aligned} \frac{RU_{Src,RCP}^{\max}}{G_{REXtoK}_{RCP}} - \frac{RU_{Src,LCP}^{\max}}{G_{REXtoK}_{LCP}} &= T_{RX_{RCP}} - T_{RX_{LCP}} \\ \frac{RU_{sky,RCP}}{G_{REXtoK}_{RCP}} - \frac{RU_{sky,LCP}}{G_{REXtoK}_{LCP}} &= T_{RX_{RCP}} - T_{RX_{LCP}} \end{aligned} \quad (3.2b.10)$$

The subtractions in Eqn. 3.2b.10 eliminate dependence on the radio source and background sky, leaving a dependence only on the receiver noise temperature. Arranging Eqn. 3.2b.10, the LCP receiver noise temperature can be written in terms of the RCP receiver noise temperature plus a correction term, again dependent only on the REX radiometer's response in REX units is Eqn. 3.2b.11.

$$T_{RX_{LCP}} = T_{RX_{RCP}} + \frac{RU_{Src,LCP}^{\max}}{G_{REXtoK}_{LCP}} - \frac{RU_{Src,RCP}^{\max}}{G_{REXtoK}_{RCP}} \quad (3.2b.11)$$

The pair of equations 3.2b.9, and 3.2b.11, provide a means to adjust the REX radiometer's calibration constants derived from solutions to the convex optimization of Eqn. 3.2.2, for the purpose of equalizing the radiometer's temperature brightness profiles such that they are consistent with an unpolarized source. The procedure, or algorithm for doing so is illustrated in Figure 3.2b.2. The RCP conversion

constant $G_{REXtoK_{RCP}}$, is perturbed by an amount ΔG , and the LCP conversion constant $G_{REXtoK_{LCP}}$, is computed using Eqn. 3.2b.9. Then the receiver noise temperatures are updated via Eqn. 3.2b.11, but averaged with the “old” values before the update. This average is done to stabilize the algorithm and suppress tendencies toward instabilities typical in iterative algorithms. The process then converts REX units to temperature and takes the temperature difference between the two polarizations, and calculates an L2 norm, the sum of the square of the differences. The RCP conversion perturbation ΔG , is varied via convex optimization to minimize the L2 norm, expecting it will vanish at least to within the statistical precision of the REX Radiometer.

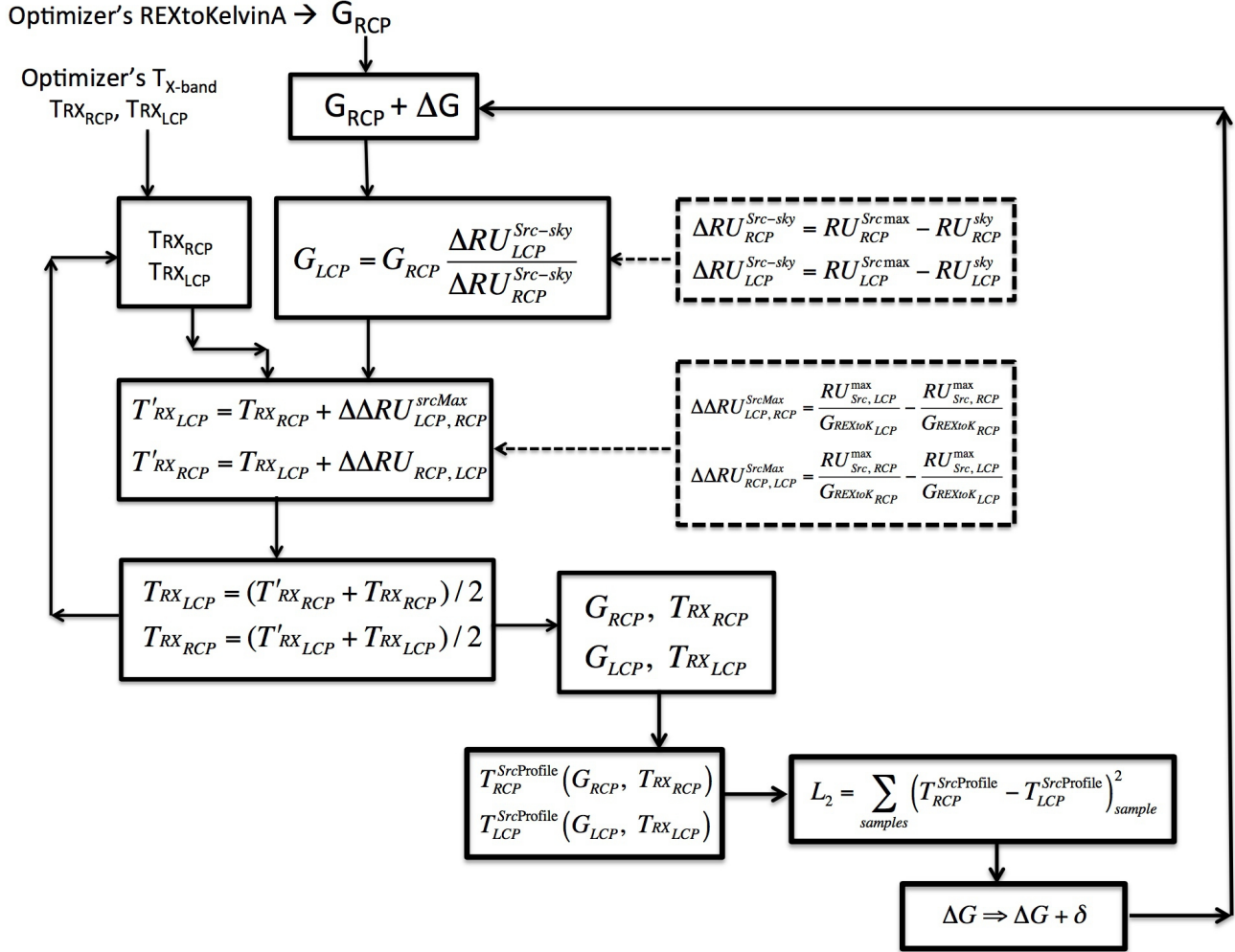


Figure 3.2b.2. Flow chart of the algorithm for balancing the calibration constants to resolve the polarization anomaly.

REX unit to Kelvin RCP	REX unit to Kelvin LCP	RCP Rx Noise Temperature	LCP Rx Noise Temperature	HGA RCP aperture efficiency	HGA LCP aperture efficiency
G_{REXtoK}	G_{REXtoK}	$T_{xb}(K)$	$T_{xb}(K)$	e_{HGA}	e_{HGA}
$84.76 \cdot 10^6$ $\pm 0.1 \cdot 10^6$	$205.26 \cdot 10^6$ $\pm 0.1 \cdot 10^6$	149.6 ± 0.1	138.8 ± 0.1	0.601 ± 0.001	0.602 ± 0.001

Table 3.2b.1. REX Radiometer Calibration Constants optimized to equalize RCP and LCP polarization measurement for REX radiometry.

The results from processing the calibration constants through the equalizing algorithm described above and illustrated in Figure 3.2b.2., are listed in Table 3.2b.1. Converting the Thermscan profiles with the revised calibration constants produces the temperature profiles in Figure 3.2b.3, for the diametric scan, and figure 3.2b.4, for the polar scan. The scans do indeed appear to be near identical. The difference between the two polarizations is included as the right side plot. The portion of the plots where the HGA enters and exits Pluto's disk are the most sensitive to difference in the polarizations, mainly due to the scan's timing where small time offsets, ~ 0.3 sec, are introduced by the spacecraft's data recording system. The profiles have been time offset to help identify and correct the time shift. The fine granularity of the time shifts is made possible by oversampling the profiles with a canonical band-limited, Fourier transform based method, and an oversampling ratio of 10x. This method guarantees exact values on the original time sample points, and produces band-limited values for the intermediate samples, (i.e. no new frequencies are introduced, unlike point-to-point interpolators)

The ensemble of time offsets of the difference between RCP and LCP, for both the diametric and polar profiles, contain one offset that reasonably appears to have a near-zero difference. Particularly, an LCP offset of -0.8 sec for the diametric profile, and an LCP offset of +0.3 sec for the polar profile, produce differences that are statistically within the fluctuations present throughout the profiles. There is however, at least one feature in both profiles that appears to be close to invariant with respect to the time offsets, indicating a persistent polarization difference. In the diametric profile, this feature is at time of ~ 100 sec, and for the polar profile the feature is at ~ 25 sec.

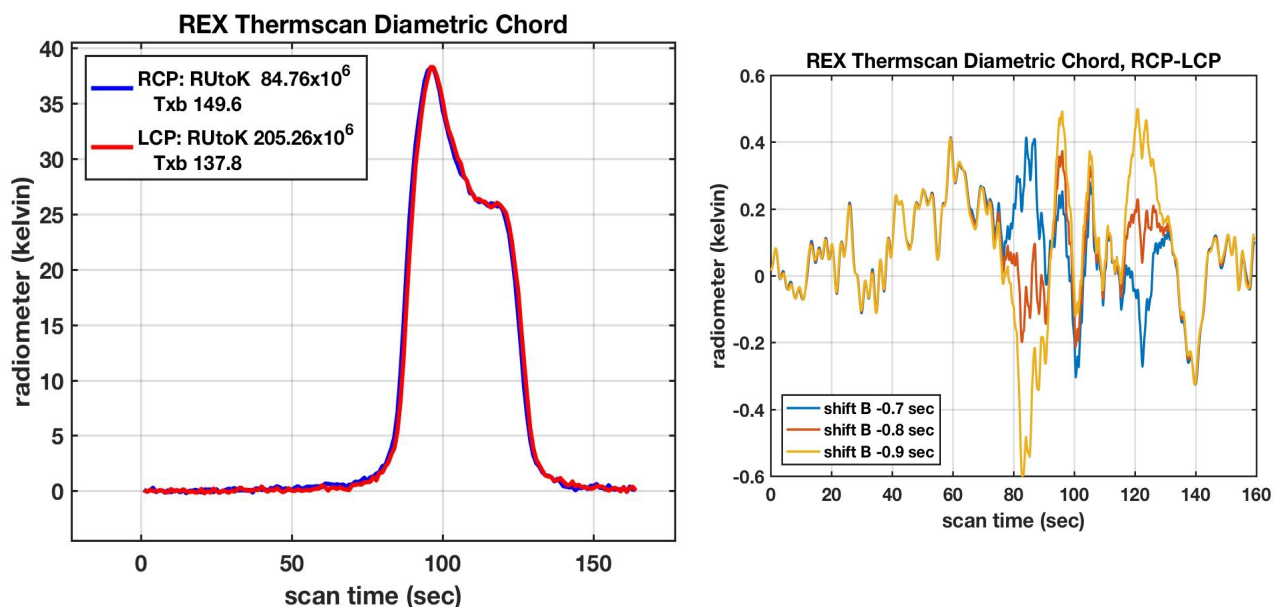


Figure 3.2b.3. REX Radiometer Scan of Pluto's Diametric chord as seen from the Spacecraft. The left side plot is the diametric chord scan in both RCP and LCP polarizations. The right side plot is the difference between the RCP and LCP polarizations for three time offsets caused by the spacecraft's recording system's time delay between the start of recording between the polarization channels.

Only one radiometric measurement of one source, the diametric scan, was used in the algorithm in Figure 3.2b.2, an algorithm based on the assumption the source was unpolarized. Using the conversion constants produced by this algorithm, as presented in Table 3.2b.1, all the other radiometer

measurements can be converted to brightness temperature and provide a critical test of the assumption that all the sources are unpolarized. The polar scan in Figure 3.2b.4, is such a test, and indeed appears unpolarized across both Pluto's disk and the background sky.

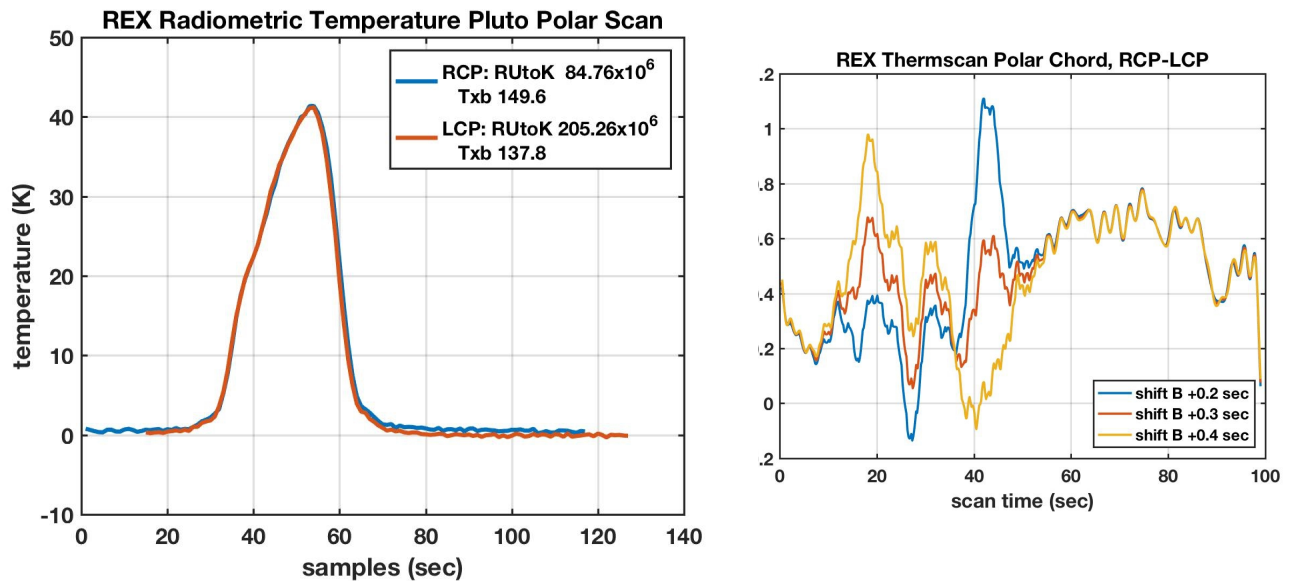


Figure 3.2b.4. REX Radiometer scan of the chord that intersects Pluto's winter pole as seen from the Spacecraft. The left side plot is the polar chord scan in both RCP and LCP polarizations. The right-side plot is the difference between the RCP and LCP polarizations for three time offsets, caused by the spacecraft's recording system's time delay between the start of recording between the polarization channels.

3.3.0 The REX Radiometer Calibration Measurements

The measured radiometric power in REX units of the radio sources are listed in Table 2.0.1. These measurements are further evaluated for radiometric calibration in the following sections: the radio background sky in section 3.3.1, the standard radio astronomy sources in section 3.4, the sun in section 3.5, Jupiter in section 3.6, and the uplinks transmitted from earth in section 3.7.

3.3.1 Radio Sky Background

Locations were found on the radio sky using sky maps from all-sky radio surveys [Condon, et.al, 1998], where the sky temperature is within a few tenth's of a Kelvin of the Cosmic Microwave Background (CMB) for a region large with respect to the HGA's beam. The HGA is a 2.1-m diameter dish, and for the X-band receiver wavelength of 4.2 cm, the 3 dB beamwidth of the HGA is 1.2 degrees. Three suitable locations were found, and are detailed in Figure 3.3.1.

Radio Source Standards

Cass-A: RA $23^{\text{h}} 23^{\text{m}} 26^{\text{s}}$, dec $+58^{\circ} 48'$
 350.8583, +58.8000

Taurus-A: RA $5^{\circ} 34' 32''$ | Dec $22^{\circ} 0.870'$
 83.6333, +22.0167

Cygnus-A: RA $19^{\text{h}} 59^{\text{m}} 28.3566^{\text{s}}$, dec $+40^{\circ} 44' 02.096''$
 299.8667, +40.7339

Cold Sky Positions

S	AZIM		ELEV		
	RA	Dec	X	Y	Z
Position A	91.20	17.9	-0.0199287	0.95138570	0.3073566
Position B	88.62	13.4	0.02342757	0.97249373	0.2317479
Position C	93.80	13.4	-0.0644697	0.97063720	0.2317479

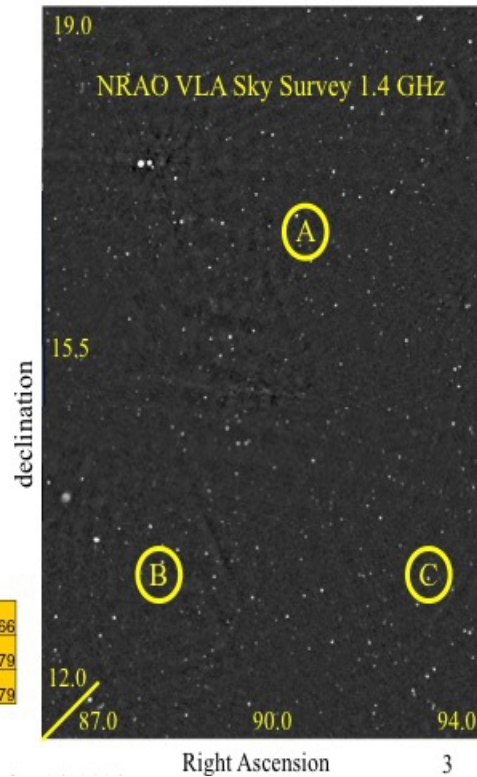


Figure 3.3.1. Cold Sky Locations used for REX Calibration. From [Condon, et al., 1998], VLF Sky Survey.

Since the CMB temperature is 2.725 K, and only half of its power is added to the receiver's own noise temperature, long acquisitions were necessary to attain the precision needed for determining the receiver's noise temperature. Observations of several hundred seconds were typical. In addition to achieving high precision of the radiometer power, sufficient integration intervals were obtained to evaluate the stability of the X-band receiver. The REX radiometer power sequences from each of the Cold Sky locations are contained in Figures 3.3.2 though 3.3.4.

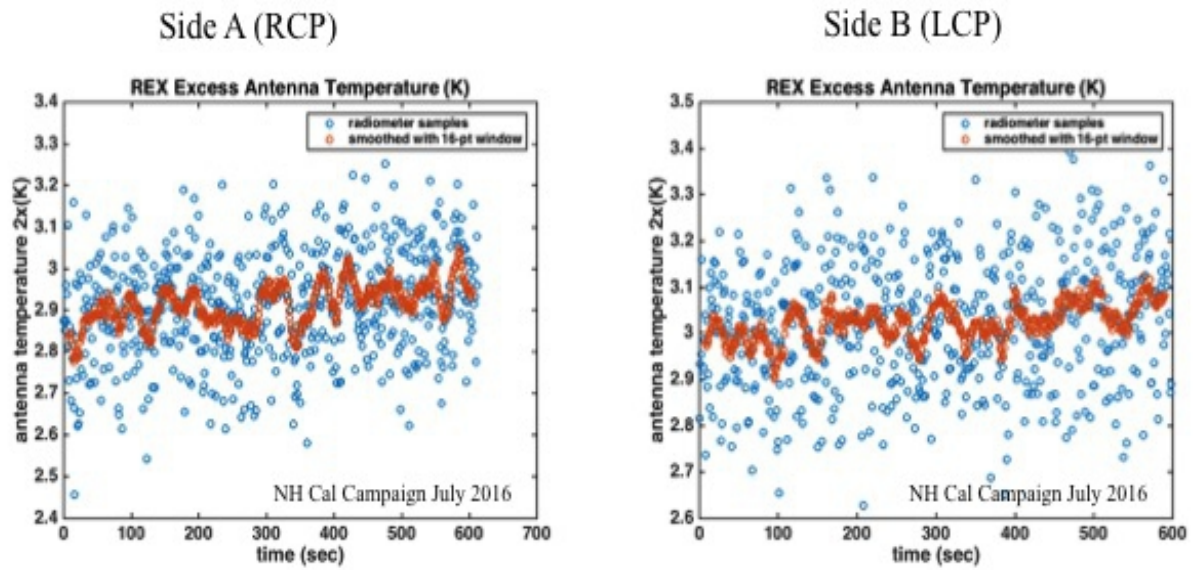


Figure 3.3.2. Cold Sky Location A, RA 91.20°, Dec 17.9°. Note: the first 200 samples (or 202.4 seconds) are Figure 2.1.1.

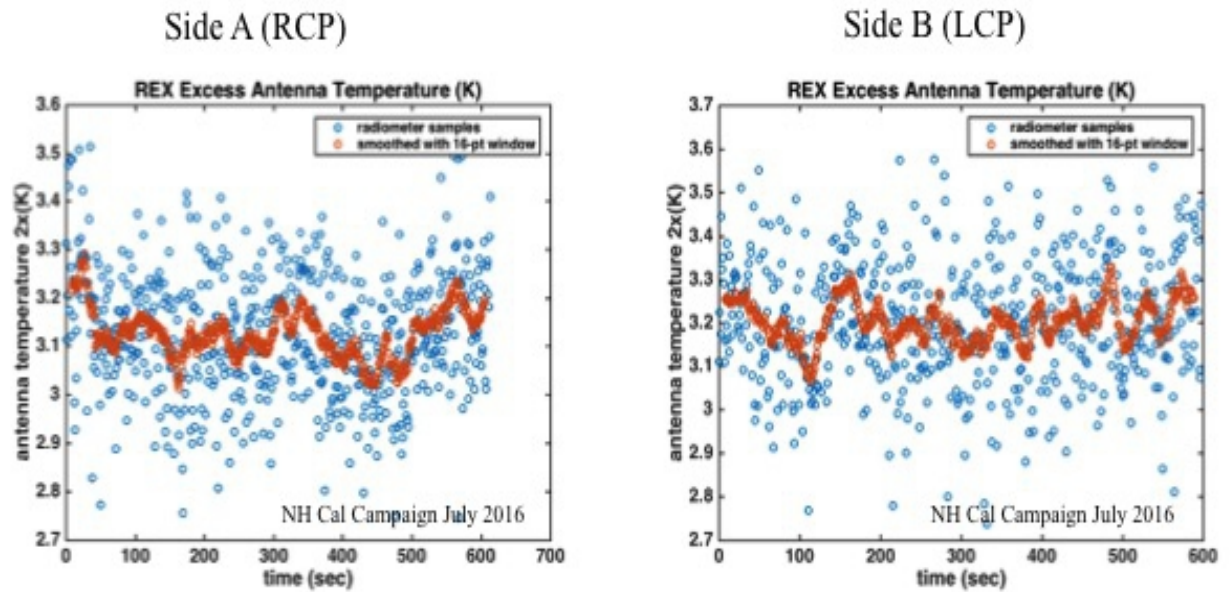


Figure 3.3.3. Cold Sky Location B. RA 88.62°, Dec 13.4°.

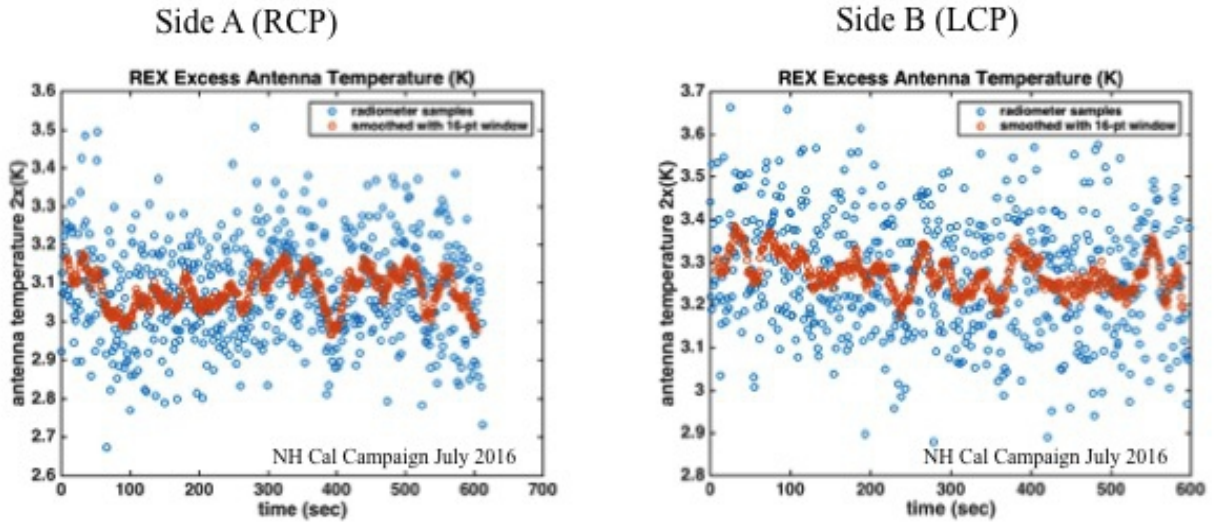


Figure 3.3.4. Cold Sky Location C. RA 93.80°, Dec 13.4°.

The power fluctuations in these six sequences form Gaussian distributions near identical with those in Figure 2.1.2. The scaling of their STD's follows the trends in Figure 2.2.2, as well. The six STD scaling, as a function of integration length, is in Figure 2.1.3. The linear trend in the log-log plot, with a slope of -1/2, confirms that the X-band receiver is sufficiently stable such that the mean of the entire sequence for each cold sky location is a reliable measure of the REX radiometer power.

Even though there are three distinct and arguably independent measurements of radiometric power from cold sky, the temperatures are so very near identical that the three locations do not qualify as three independent constraints for purposes of solving for the REX radiometer calibration constants. On the other hand, these are three independent total power integrations, and they are three statistically independent samples of radiometric power. Thus there is an opportunity to check if the three are statistically consistent, and if the gain variations are suitably small, and the temperature of the three cold sky locations is indeed the same within the expected variation.

The relationship between the measured radiometric power and the calibration constants in Eqn. 3.1.1, indicates that if either of the constants are known, the other is determined by the measurement. For example, with apriori knowledge of the receiver's noise temperature T_{RX_P} , the REX units to Kelvin conversion constant is found using Eqn. 3.1.1. In particular, from Table 3.1.1, with T_{RX_RCP} , is 144 K, and T_{RX_LCP} , is 146 K, then the REX units to Kelvin conversion constants are,

$$G_{REXtoK_P} = \frac{RU_{ColdSky n, P}}{\frac{1}{2}T_{ColdSky n, P} + T_{RX_P}} \quad (3.3.1)$$

Table 3.3.1, contains the conversion constants determined by Eqn. 3.3.1, for the three cold sky locations and the two receiver polarizations, valid for an initial choice of X-band receiver noise temperature, $T_{RX_RCP} = 144$, and $T_{RX_LCP} = 146$. The receiver noise temperatures will be reevaluated using the full suite of calibrators in Section 4. But the revised noise temperatures will be close enough that a comparison in Table 3.3.1 among the cold sky sources is meaningful.

<i>RCP</i>	Cold Sky A	Cold Sky B	Cold Sky C	Off Sun*
Radiometer (10^9 REX units)	12.852	12.861	12.859	12.880
STD (10^6 REX Units)	1.315	1.757	1.468	1.685
REX to Kelvin (10^6 REX units/K)	88.180 +/- 0.008	88.242 +/- 0.012	88.228 +/- 0.009	88.372 +/- 0.015

<i>LCP</i>	Cold Sky A	Cold Sky B	Cold Sky C	Off Sun*
Radiometer (10^9 REX units)	28.883	28.901	28.907	28.815
STD (10^6 REX Units)	2.705	3.0216	2.585	2.451
REX to Kelvin (10^6 REX units/K)	195.224 +/- 0.018	195.341 +/- 0.020	195.384 +/- 0.016	195.027 +/- 0.030

Table 3.3.1. REX Radiometer Conversion from Cold Sky Measurements. Tables are separated by RCP and LCP. Errors in the table are the combined statistical STD's of the mean radiometer power and the uncertainty introduced by the two solar calibrations. *Note: The Sun is included in the last column is not the radiometric power from the sun, but rather from the background sky (RA, dec), during a REX measurement from the Cal Campaign in 2016.

Comparing the values in the last row of Table 3.3.1, for statistical consistency, the conversion constants for Cold Sky are not within 1 sigma of each other indicating the sky temperature differed from location to location. This is the case for both polarizations. Most likely the sky temperature of location A, was the 2.7 K expected for the temperature of the CMB, but for the other two locations the temperature was higher by ~ 0.3 K.

The statistical consistencies are further illustrated in Figure 3.3.5, where the three Cold Sky locations are plotted along with their respective 1 sigma error bars due to the STD of the measurements. There is a systematic component to the uncertainties from the yet unresolved values of the receiver noise temperatures. However, these systematics will shift the ensemble of the points vertically in Figure 3.3.5.

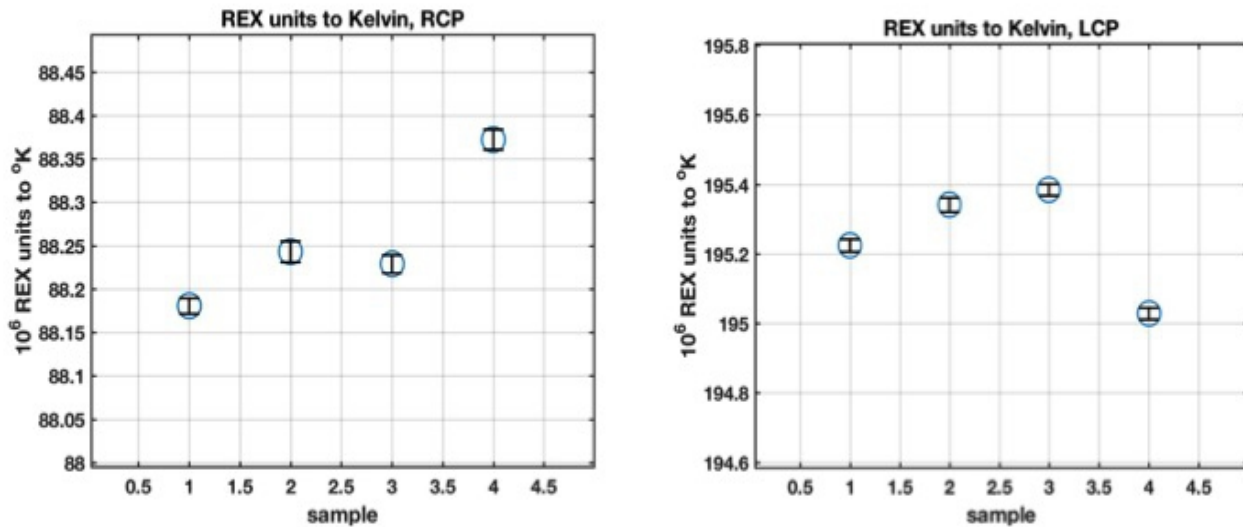


Figure 3.3.5. Comparison of the “REX units to Kelvin” estimates for the three Cold Sky locations with the “REX units to Kelvin” solution based on a priori knowledge of the receiver's noise temperature.

3.4 Standard Radio Source Power Measurement

Four additional radio source standards have been measured by REX and New Horizons for the purpose of radiometric calibration. These measurements were scans using the HGA and performed during spacecraft commissioning in 2007, and during the July 2016 Calibration Campaign. The measurements consisted of cross-hair scans by the HGA from an extent two degrees on either side of the radio source's center. The four radio sources measured were, (1) Cass-A, (2) Taurus-A, (3) Cygnus-A, and (4) Virgo-A, which are among the brightest radio sources on the sky. Their radio flux in X-band is low, but still strong enough to constrain estimation of the REX calibration constants. Figure 3.4.1, shows the radio flux expected from these standard sources over a range of radio frequencies near X-band, using radio flux models from published archival observations, e.g. [the HEASARC survey], [Perley, 1984], and [Rebold 1988]. The flux density from the supernova remnant Cass-A decays with an index [Vinyaiken 2014], that was used to predict the radio flux at the time of the REX measurements during commissioning in 2007.

The standard radio sources distinguish themselves from the cold sky locations in that the radio sources are compact, i.e. nearly point sources on the sky, and do not fill the beam of the HGA. In contrast, the cold sky locations are broad, beam-filling regions at ~ 2.7 K. To obtain an equivalent temperature for the point sources, the RF flux

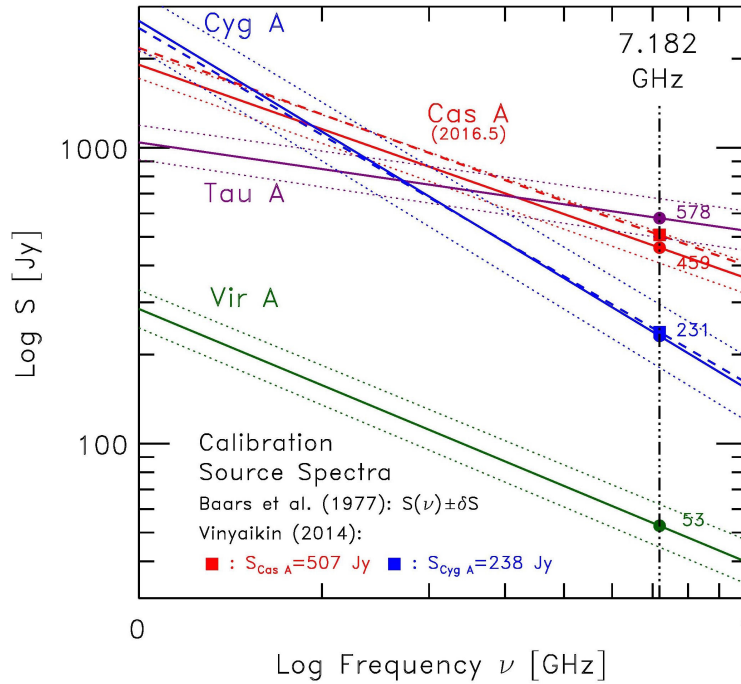


Figure 3.4.1. Radio Flux Models of Standard Radio Sources. More recent flux densities for Cyg A and Cass A were determined by Vinyaikin (2014), and incorporated here.

density from the radio source Φ_S , is presumed to uniformly illuminate the HGA, and the gain of the HGA, or equivalently the HGA's effective aperture A_{HGA} , is needed to estimate the RF power, $P_{RF S}$ in the X-band receiver from the illuminating RF flux. The RF power in the X-band receiver is represented by an equivalent temperature T_S , chosen such that, $P_{RF S} = k T_S$, k is Boltzmann's constant. The RF power in the X-band receiver is the radio flux integrated over gain profile of the HGA, or alternatively, the product of the radio flux and the equivalent aperture of the HGA.

$$kT_S = A_S + \Phi_S + kT_{sky} \quad (3.4.1)$$

Knowing both T_S , the equivalent temperature of the radio source, and the sky temperature, and using the process outlined in Section 3.3, and with an equation similar to (3.3.1), the REX radiometer calibration constants can be independently determined. In this case, Eqn. 3.3.1, becomes,

$$G_{REXtoK-P} = \frac{RU_{S_{n,P}}}{\frac{1}{2}T_{S_{n,P}} + T_{RX-P}} \quad (3.4.2)$$

where $RU_{S_{n,p}}$ is the REX Radiometer's units, and $T_{S_{n,p}}$ is the thermal brightness temperature estimated from the flux.

The radio source standards provide an independent determination of the calibration constant, again subject to a priori knowledge of the receiver's noise temperature.

The radiometric power measured with REX for the standard sources chosen for calibration is shown in Figures 3.4.2 to 3.4.4. Typically, the radio sources are not point-sources imbedded in a uniform background of cold sky. Most are galactic plane objects, and the scan geometry produced an asymmetric background. The scans were orthogonal cross-hairs, oriented using published radio sky images to resolve the asymmetry. The result is able to estimate the peak RF power relative the background power. The scans in Figures 3.4.2 to 3.4.4 are radiometric power in REX units.

REX Radiometer XY-scans across Radio Source A
(Taurus A)

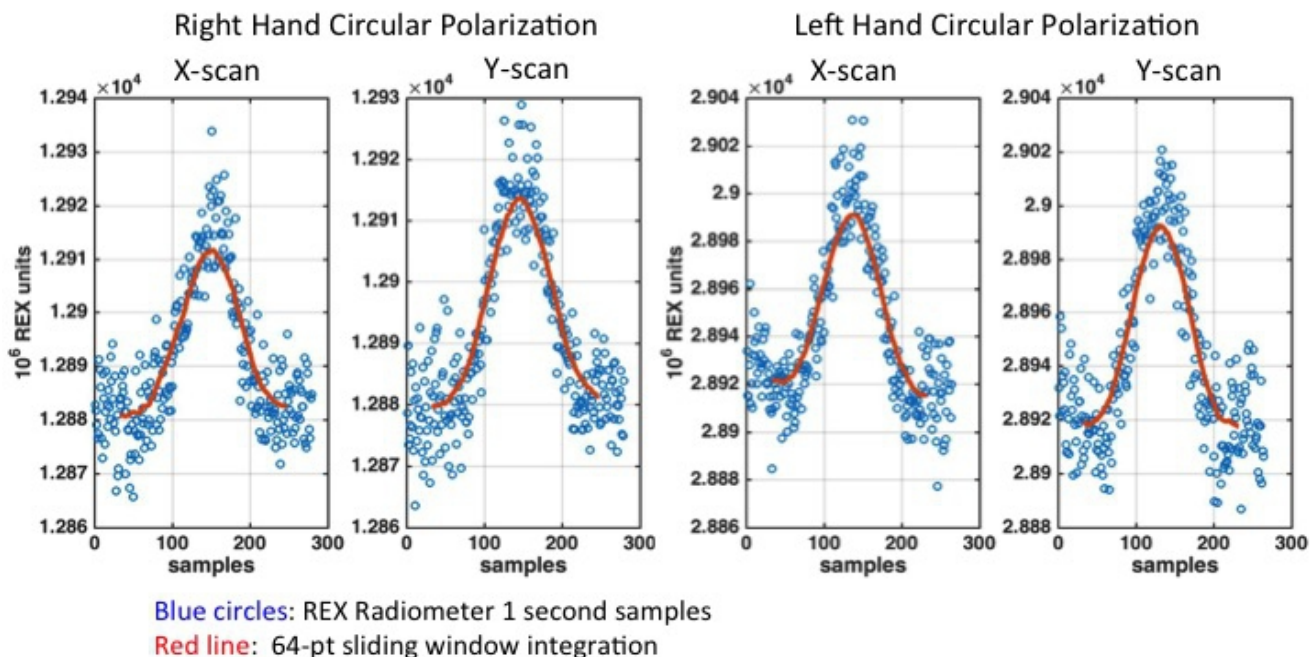


Figure 3.4.2. Scans Across Standard Radio Source Taurus-A.

REX Radiometer XY-scans across Radio Source B
(Cass A)

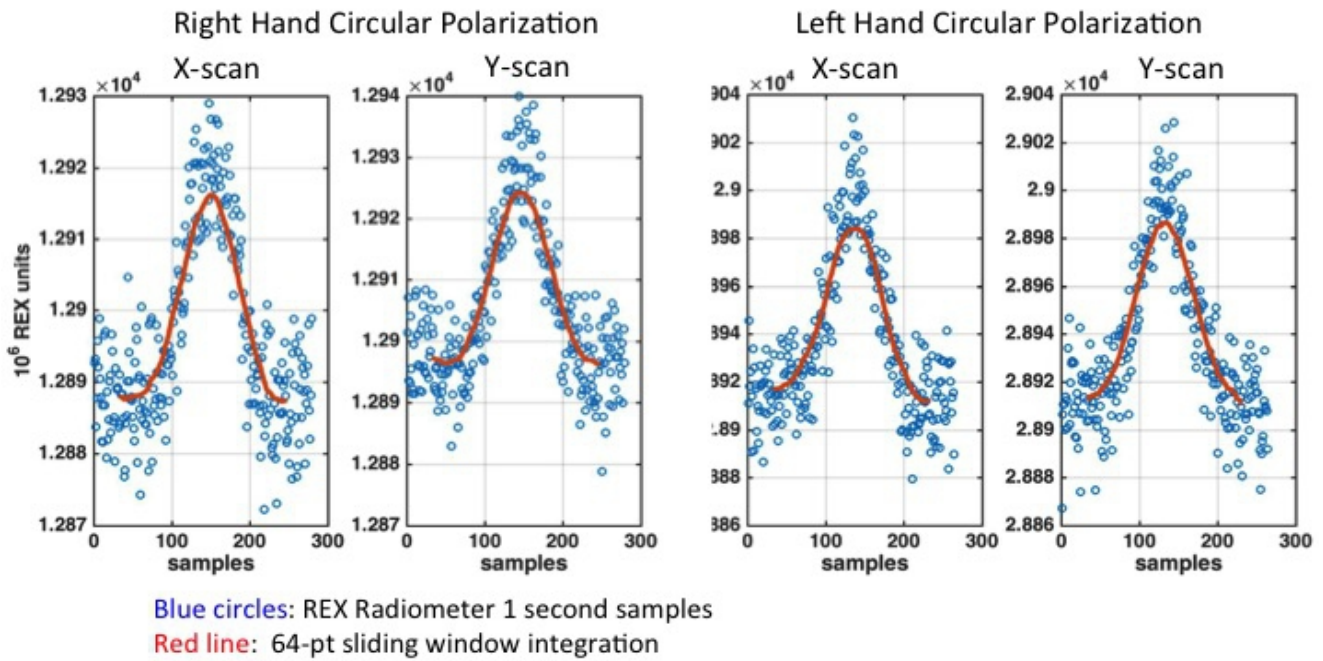


Figure 3.4.3. Scans Across Standard Radio Source Cass-A.

REX Radiometer XY-scans across Radio Source C
(Cygnus A)

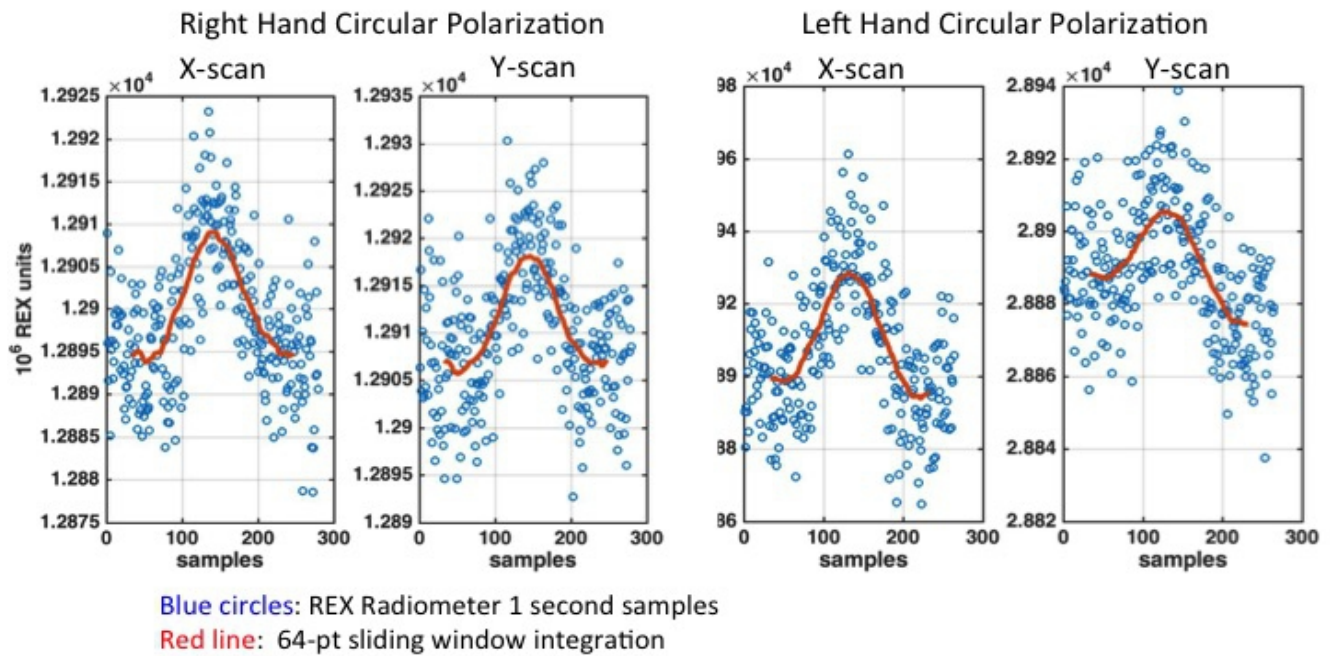


Figure 3.4.4. Scans Across Standard Radio Source Cygnus-A.

The equivalent temperature for the point sources is determined from the enhancement in REX power at the maximum of the scan above the power at the edges of the scan. Using the known flux densities in Jy, and the ratio of REX units to Janskys, and scaling REX units to Kelvin via the HGA's effective aperture A_{HGA} , the equivalent temperature of the source is computed. The REX radiometer power for each source is plotted in Fig. 3.4.5. as a function of the known flux density.

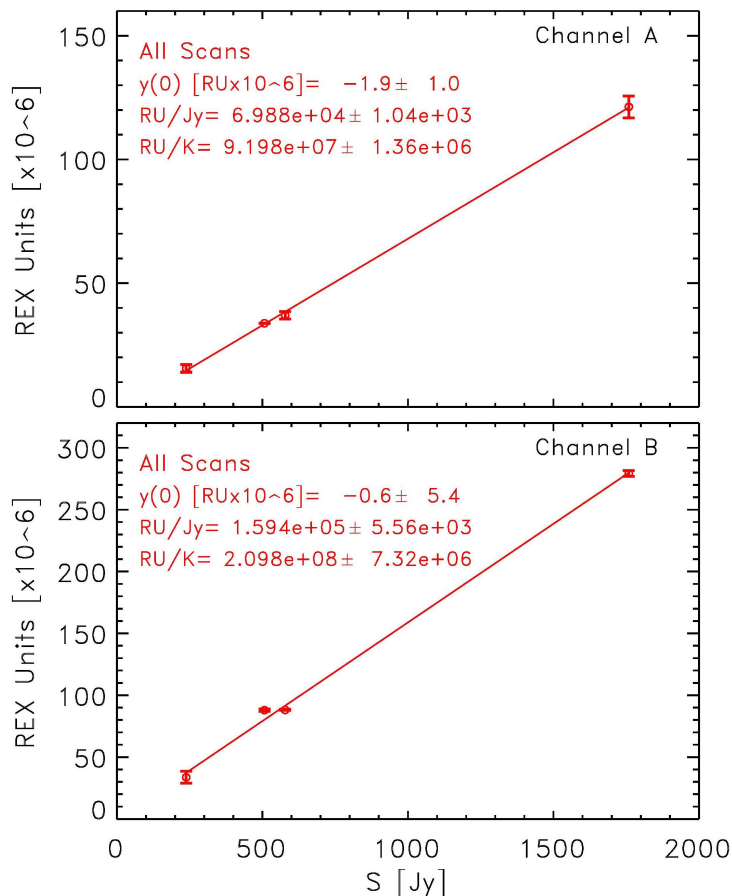


Figure 3.4.5. REX observed power for four known radio sources (upper plot: Channel A; lower plot: Channel B) The points from left to right are for Cyg A, Cas A, Tau A, and the Sun, respectively. The observed increase in radio power (REX units) is plotted versus the known flux density of each source in Jy. The slope of each least-squares fit to the observations, shown in each panel, is the scaling factor for RU/K.

A useful sense of consistency is to convert the REX units of the radio source standards to equivalent temperature using apriori knowledge of the receiver's noise temperature and a version of Eqn. 3.4.2,

$$T_{S_{n,P}} + = 2 \left[\frac{RU_{S_{n,P}}}{G_{REXtoK_P}} - T_{RX_P} - T_{sky} \right] \quad (3.4.3)$$

The antenna temperature estimates $T_{S_{n,p}}$ found with Eqn. 3.4.3, are plotted in Figure 3.4.6, with the equivalent temperature from the radio flux on the horizontal axis, and the computed temperature from REX units on the vertical axis. The effective aperture of the HGA that gives the best agreement between the REX radiometric brightness and the effective antenna temperature of the standard radio sources, is 0.6.

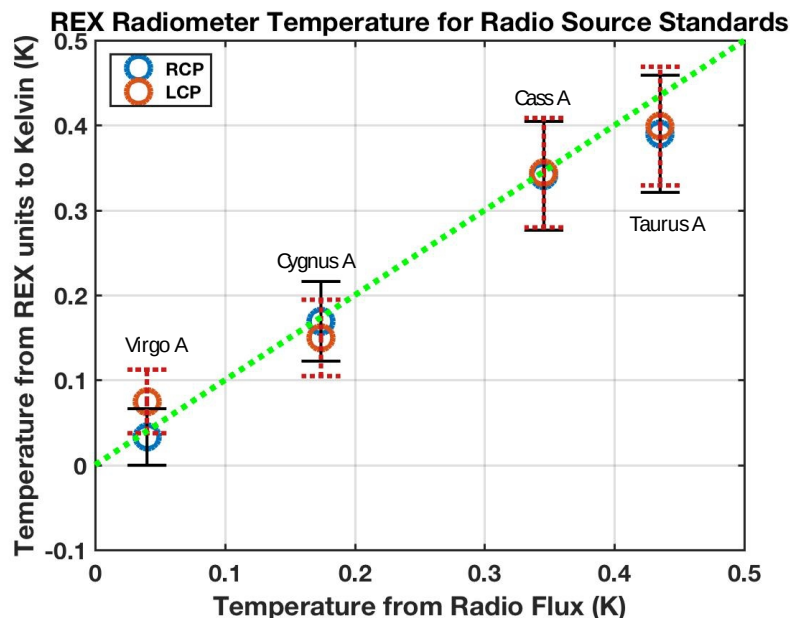


Figure 3.4.6. Temperature to Temperature Comparison for Standard Radio Sources. The radio brightness temperature estimated from the radio source standard's flux is the horizontal coordinate. The vertical coordinate is the radio brightness temperature extracted from the REX radiometer. The blue markers are for the Right Hand Circular polarization measurements (RCP), and the red markers are for the Left Hand Circular polarization measurements (LCP).

3.5 The Sun as a Calibrator

During the radio occultation of Pluto four uplinks were transmitted from Earth and recorded by REX as Pluto crossed the line of sight from the spacecraft to Earth. The Earth was near-solar opposition during the Pluto Encounter as seen by the spacecraft. The angle between the Earth and the Sun was 0.23° . The uplink signal was recorded well before occultation ingress, and REX recording continued between occultation ingress and egress even though the uplink was absent in the receiver. The recording continued additionally well after egress. Just before egress, with the uplink still occulted by Pluto, the Sun appeared from behind Pluto's limb and was within the beam of the HGA for about one minute before Earth and its four uplinks again appeared. Accordingly, the Sun presented itself as a serendipitous calibrator. The REX radiometer power profile during Pluto Occultation is shown in Figure 3.5.1, with a zoomed-in version in Figure 3.5.2. Here the appearance of the Sun is evident against the decreasing power from Pluto's dark side.

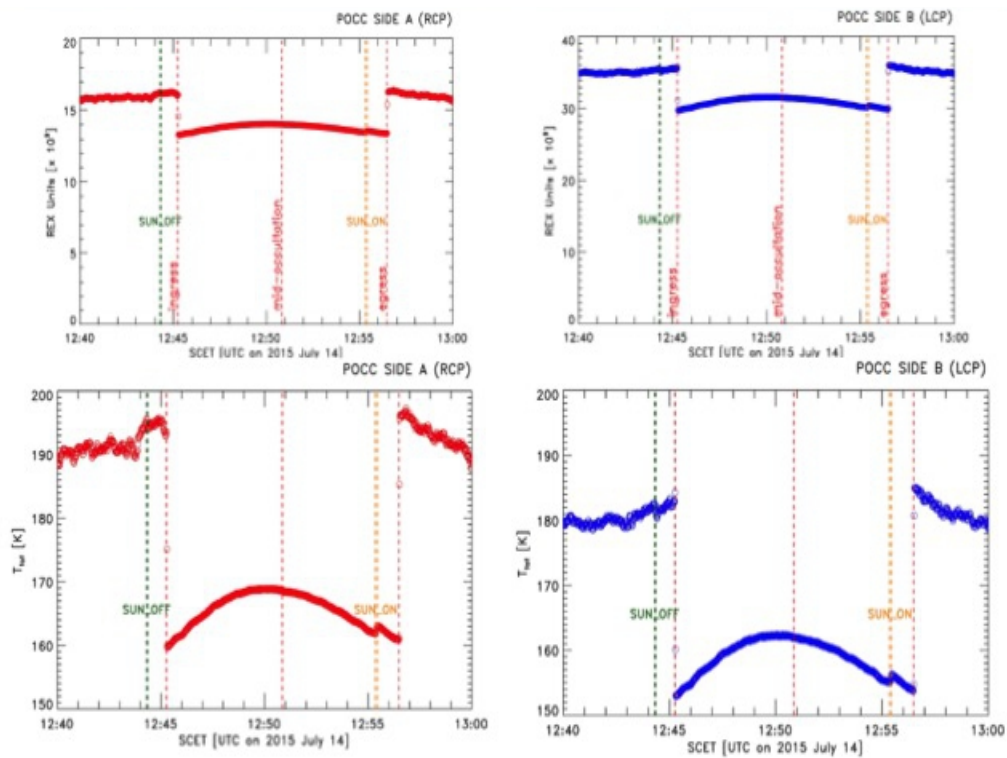


Figure 3.5.1. REX Radiometer Power during Pluto Occultation. Upper panels: Total recorded power in REX units (left: RCP; right: LCP). Lower panels: Total recorded power converted to kelvin (left: RCP; right: LCP).

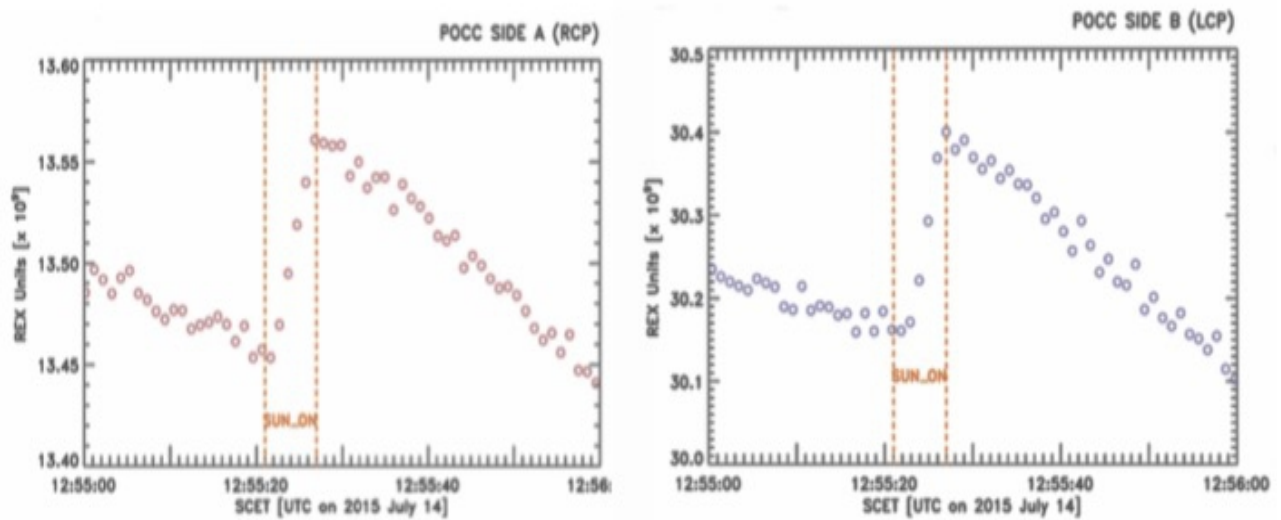


Figure 3.5.2. REX Radiometer Power During Pluto Occultation. The Sun's increase in the power just after egress (detail for the time 12:55 to 12:56 UTC). The power increases abruptly as the Sun emerges from behind the Pluto disk just before radio occultation egress.

The Sun in X-band as seen from the Earth is a strong radio source (1.5 Mjy), [Benz 2009; Ho et.al., 2008], but at the distance to Pluto of 32.91 AU, the Sun is much weaker, with a flux density of 1759 jy. Even so, the sun's antenna temperature in X-band is ~ 1.3 K, (per polarization), comparable but stronger than the radio source standards in the previous section. Although the Sun's radio power is not stable, the solar variation is very closely monitored from Earth. The variation of solar flux density occurs on timescales of hours to days.

The solar intensity was estimated from daily observations at 10.7 cm wavelength (2800 MHz) at the Dominion Radio Observatory (DRAO) in British Columbia [<http://www.spaceweather.ca/solarflux/sx-en.php>]. Using a model of solar power variation, [e.g. Zirin 1991], the solar flux density at X-band was estimated for the time of the Pluto occultation. Using a high fidelity model of solar power variation, scaled to X-band frequencies, the Sun's antenna temperature in the REX observations was estimated at the time of Pluto occultation egress.

In addition to the serendipitous detection of the Sun during Pluto occultation, a second measurement of solar radio flux occurred in the post-Pluto Encounter Calibration Campaign in July 2016, a year after Pluto Encounter. The earth was again near solar opposition, but the Sun was observed against a cold sky background. This scan is shown in Figure 3.5.3.

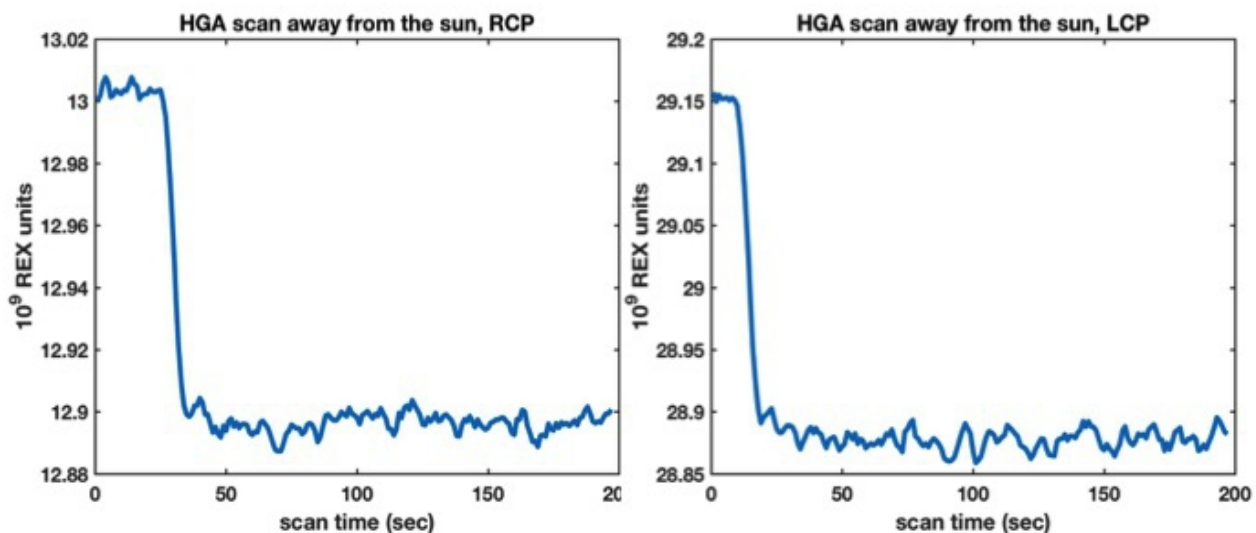


Figure 3.5.3. Scan away from the Sun during the REX Calibration Campaign, August 2016.

The REX radiometer power in Figure 3.5.3, is 13.003×10^9 , REX units for RCP, and 29.155×10^9 REX units for LCP. Attributing this increase to the combined receiver noise temperature and the RF temperature of the sun, the receiver noise temperature can be eliminated and the scaling between REX units and Kelvin is:

- REX RCP: 88.87×10^6 REX units per degree K
- REX LCP: 196.59×10^6 REX units per degree K

The antenna temperature of the Sun for the above conversion constants was 3.8 K.

3.6 Calibration of REX using Thermal Emission from Jupiter

New Horizons was launched on January 19, 2006, and encountered Jupiter on February 28, 2007, thereby receiving a gravity assist that significantly reduced the duration of the cruise to Pluto. The proximity to Jupiter afforded an opportunity to record Jupiter's thermal emissions using REX. Four days before Jupiter closest approach, the spacecraft's High Gain Antenna (HGA), was scanned diametrically across Jupiter's equator, and four days after closest approach the HGA scanned Jupiter again diametrically, from pole to pole. Jupiter's apparent size as seen from the spacecraft was 1.15° for the arrival scan, and 0.89° for the departure scan, both of which were slightly smaller than the 3 dB beamwidth of the HGA (1.2°). This proximity was especially significant, for at no other time in the Mission, other than at the Pluto Encounter itself, would a strong radio source fill nearly all of the beamwidth of the HGA, and present as high a radiometric temperature for the purposes of calibration.

The scan profiles from the REX Radiometric samples, (cadence of 1 radiometer sample per 1.024 seconds) are shown in Figures 3.6.1. From the perspective of New Horizons, the first (equatorial) scan, Jupiter was against the background sky 5 degrees above the Galactic Plane, while for the second (polar) scan, Jupiter's background was well above the Galactic Plane and in Cold Sky.

These are the scan specifics.

JREXCAL Scans

JREXCAL01 Done on February 24, 2007, start at 02:55:56 SC UTC, MET 0034591678

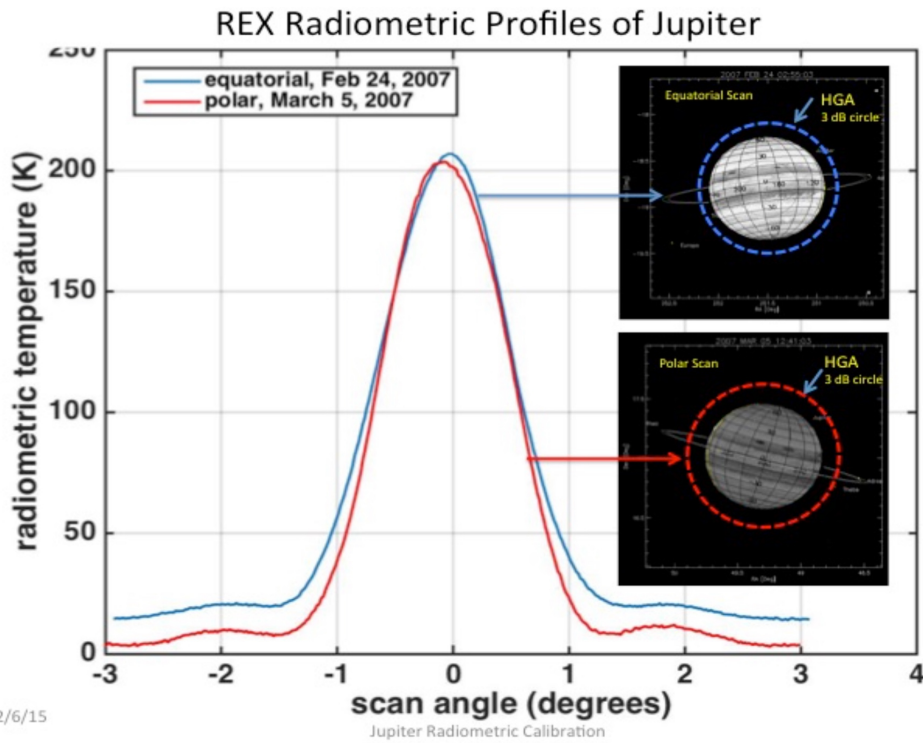
Scan from -x to +x (SC coords), and -3 deg to +3 deg Note: SC HGA boresight is in +Y Jupiter at: RA 251.5 deg, dec -18.75 deg, (16:45, +17.0)

Galac1c: 0 deg, +15 deg (close to Galactic Plane) Jupiter target angle: 19.563 mrad (full)

JREXCAL02 Done on March 05, 2007, start at 12:08:00 SC UTC, MET 0035402400

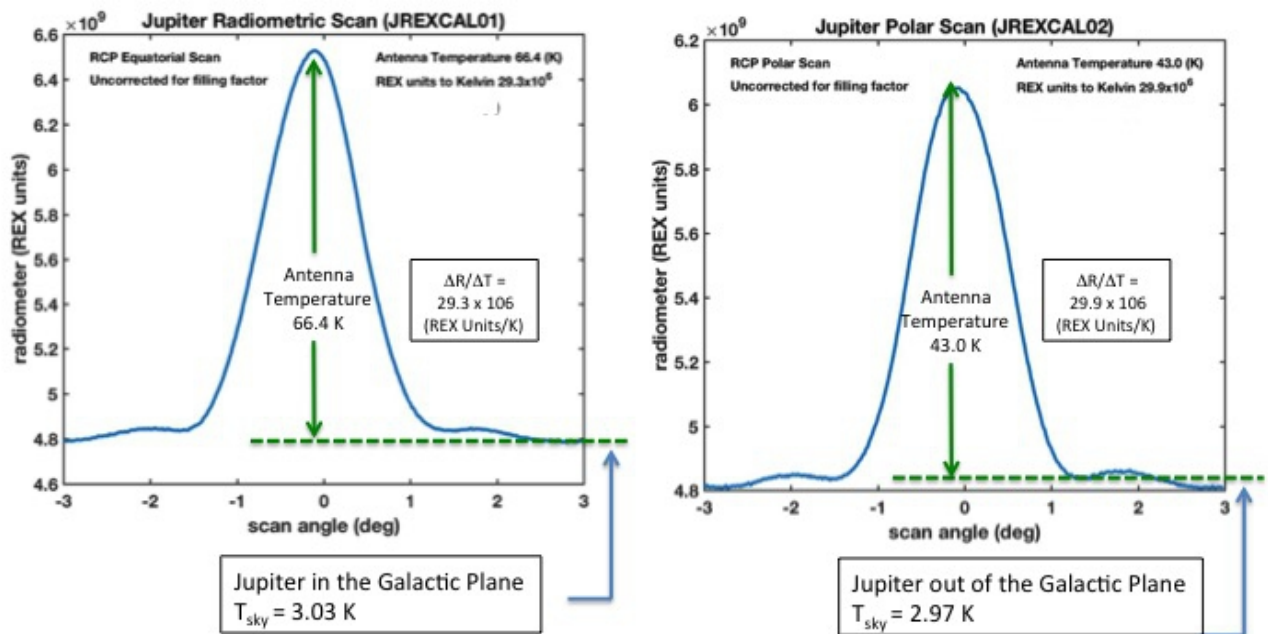
Scan from -z to +z (SC coords), and -3 deg to +3 deg Note: SC HGA boresight is in +Y Jupiter at: RA 49.25 deg, dec +17.0 deg, (03:15, +17.0)

Galac1c: 170 deg, +35 deg (well above Galactic Plane) Jupiter target angle: 15.594 mrad (full)



2/6/15

Figure 3.6.1. REX Radiometric brightness temperature scans of Jupiter with REX and the HGA. The equatorial scan is in blue, and the polar scan is in red. The inset shows a comparison between the size of the Jovian disk and the 3 dB beamwidth of the HGA.



2/6/15

Jupiter Radiometric Calibration

2

Figure 3.6.2. REX Radiometric scans of Jupiter. The ordinate is in REX units.

The gain of the HGA, or alternatively, the response of the HGA as a function of illumination direction, represented in Figure 2.3.1, is approximately circularly symmetric. The HGA gain is a strong function of the angle from the central direction (called the HGA boresight). The illumination of radio frequency power on the HGA is the integration of the radio brightness of the target as a function of illumination direction multiplied by the response of the HGA in that direction. This integration is expressed compactly as the convolution of the HGA's gain response $H(\theta, \phi)$ with the target's radio brightness angular distribution $T_J(\theta, \phi)$, in this case it is Jupiter.

$$T_{ant} = H * T_J \quad 3.6.1$$

If Jupiter were larger than the beam size of the HGA, then the HGA's antenna temperature would be Jupiter's radio brightness temperature integrated throughout the HGA's aperture. But Jupiter was somewhat smaller than the HGA's beam size.

If the HGA's gain response were constant out to some critical angle Θ_{beam} , and then zero at larger angles than that, then the HGA's antenna temperature would be the integral of the fraction of the HGA's beam occupied by Jupiter, η , at Jupiter's temperature T_J , plus the remaining fraction of the HGA's beam not occupied by Jupiter $(1-\eta)$ at the temperature of the background sky T_{sky} , as expressed in Eqn 3.6.2, with the additional assumption that the thermal emission from Jupiter is constant over its disk.

$$T_{ant} = \eta T_J + (1 - \eta) T_{sky} \quad 3.6.2$$

The filling fraction, η , is the fraction of the HGA's beam area occupied by Jupiter as the radiometric target. Since the convolution in Eq'n 3.6.1, is a linear operator, it can be reorganized in terms of Θ_{beam} , under the earlier assumption T_J is uniform over its projected surface.

$$\begin{aligned} I(\theta, \varphi) &= \int_0^{2\pi} H(\theta, \varphi) T(\theta, \varphi) d\varphi \int_0^\pi \sin(\theta) d\theta \\ &= \left[\int_0^{2\pi} H(\theta, \varphi) d\varphi \int_0^\pi \sin(\theta) d\theta \right] \left[\int_0^{2\pi} T(\theta, \varphi) d\varphi \int_0^\pi \sin(\theta) d\theta \right] \\ &= \left[\int_0^{\Theta_{beam}} \tilde{H}(\theta) \sin(\theta) d\theta \right] \bar{T} \\ &= \pi \Theta_{beam}^2 \bar{T} \end{aligned} \quad 3.6.3$$

Here Jupiter's temperature distribution is replaced with the average over the projected surface, and the integral of the HGA's gain is replaced by the area of a circle whose radius is the equivalent angular width of the HGA's gain, using the equivalence,

$$\begin{aligned} G &= \int_0^{2\pi} H(\theta, \varphi) d\varphi \int_0^\pi \sin(\theta) d\theta \\ &= \int_0^{\Theta_{beam}} \tilde{H}(\theta) \sin(\theta) d\theta \\ &= \pi \Theta_{beam}^2 \end{aligned} \quad 3.6.4$$

Where,

$$\tilde{H} = H/H(0,0)$$

Both the beam shape of the HGA and the shape of Jupiter are very nearly circular, hence η is well represented by the ratio of the area of two circles with angular diameters Θ_{beam} , and Θ_J . for the HGA and Jupiter respectively.

$$\eta = \left(\frac{\pi \Theta_J^2 / 4}{\pi \Theta_{beam}^2 / 4} \right) = \left(\frac{\Theta_J}{\Theta_{beam}} \right)^2 \quad 3.6.5$$

Jupiter size was determined from the navigation solution for the spacecraft's trajectory, obtaining the distance to Jupiter at the time of the radiometric scans, and the corresponding angular diameters of Jupiter for both scans.

The effective angular area of the HGA beam is a circle whose angular diameter is 1.60 degrees, the asymptotic limit of the integral in Eqn. 3.6.4. This integral is shown in Figure 3.6.3. as a function of the upper integration limit.

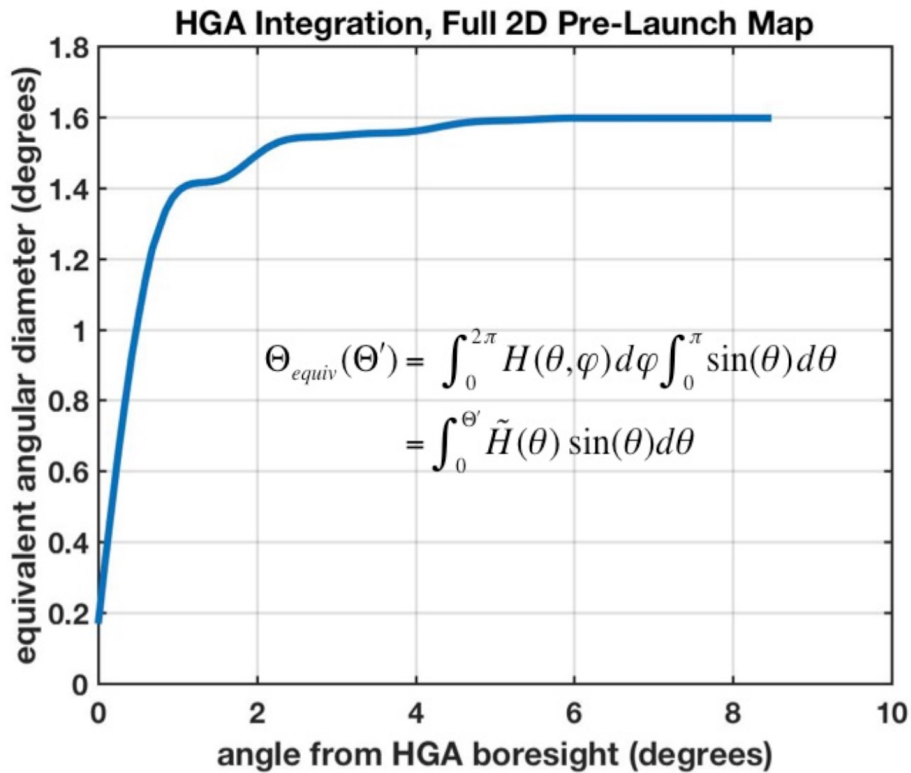


Figure 3.6.3. Equivalent HGA angular diameter integral, using the pre-launch angular response of the HGA [Schulze 2017].

Using the equivalent HGA angular aperture from Fig. 3.6.3., the conversion constants of REX units to Kelvin and the X-band Receiver's noise temperature are derived for the two Jupiter radiometric scans. The derivation relies on knowledge of the background sky temperature, and the filling fraction, itself dependent on the distance to Jupiter. This distance relies on information from spacecraft navigation that has small uncertainties. Consequently, an optimization was constructed that allowed for the small uncertainties in the background temperature and the uncertainties in the distance to Jupiter.

The optimization was a 4-dimensional parameterization, with two dimensions for each of the two scans. Particularly it allowed the two sky temperatures to vary 0.3 K near 2.7 K, and the filling fractions to vary within a few percent. The optimization derived both calibration parameters, the REX units to Kelvin conversion constant, and the receiver noise temperature. An L2 metric was used as the square of the Rx noise temperature difference added to the square of the REX-to-Kelvin difference. A weight was included penalizing large changes in the search parameters. The optimizer found good solutions for the HGA equivalent aperture diameter, with sky temperatures differing only 0.003 K from 3.0 K, and filling fractions larger by ~10%, implying Jupiter was either a mismatch in the estimated sizes of Jupiter and the HGA, or the assumption attributing Jupiter's radio flux as entirely thermal emission.

The behavior of the derivation is shown in Figure 3.6.4, where the optimization objective was to find solutions such that both the conversion constant and receiver noise temperature are the same for both scans.

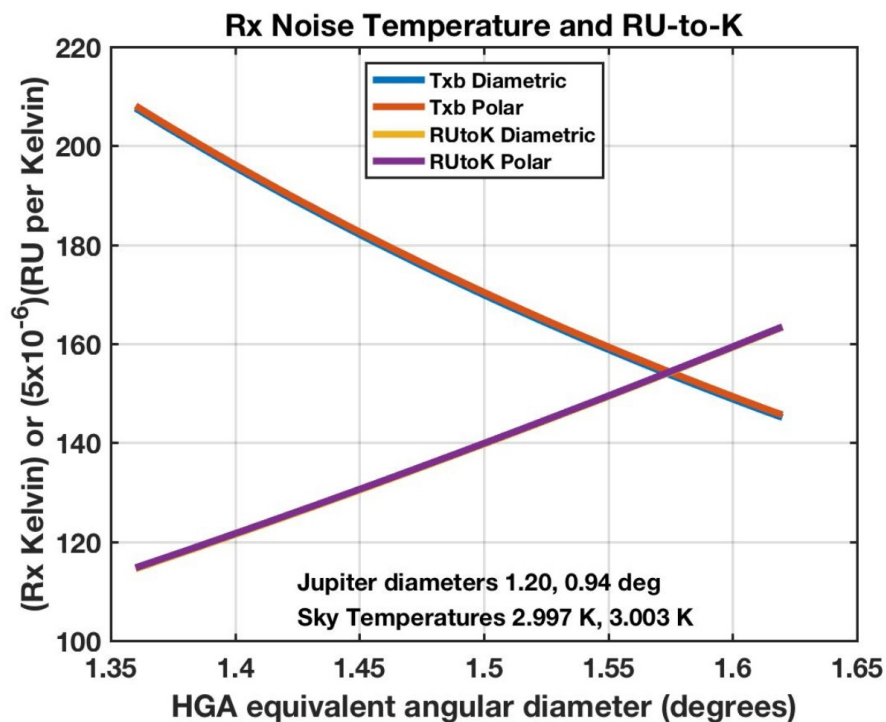


Figure 3.6.4. X-band Receiver Noise Temperature and REX units to Kelvin conversion constants for the Jupiter Equatorial and Polar Radiometric Scans. The plot pairs representing the two Jupiter scans are visually coincident, indicating the success of the optimizations. The equivalent angular diameter of the HGA was variable, i.e. the optimization was run for each choice of the HGA equivalent angular diameter as a means of validation.

An equivalent angular diameter of 1.52 degrees, for the HGA, results in an X-band Receiver noise temperature of 144 K, and a conversion constant of 33.2×10^6 . Unfortunately, the receiver gain setting changed during the course of the mission with the consequence of changes in the conversion constant. A calibration campaign was performed post Pluto encounter to determine the REX units conversion constants and the receiver temperatures. The post encounter calibration and results are in Sections 3.0, 3.1 and 3.2.

3.7 Calibration Using X-band Uplinks from Earth

Over the course of the New Horizons mission unmodulated X-band uplinks were transmitted from Earth using DSN stations to the New Horizons spacecraft. These uplinks were received in the spacecraft's X-band Receiver and recorded using REX. The REX process converted the uplink signal to a 1.25 kHz baseband in both in-phase and quadrature channels, and Nyquist sampled those channels at 1250 samples per 1.024 seconds. The uplink's frequencies were offset from band center (i.e. DC), by +/-100 Hz, such that the uplink's cross-polarization signals were well separated within their respective channels.

The X-band power in the uplink signal at the spacecraft used a pre-launch link analysis calibration, that has agreed with observation to within +/-0.1 dB, over the duration of the mission.

With knowledge of the uplink's X-band power, and the uplink recordings produced by REX, an alternative estimate of the spectral power density of the X-band receiver's noise can be derived. By taking FFT's of successive 1250-sample sequences of the in-phase (I) and quadrature (Q) samples, the mean spectral power density of both the uplink and the X-band receiver's noise is estimated to a statistical precision of 0.01 dB or better. These estimates are obtained for every uplink recorded by REX during the New Horizons mission.

An example of this process is shown in Figure 3.7.1, for both RCP and LCP uplinks recorded two days after the Pluto Encounter. Notice that the SNR of the RCP uplink is 4.9 dB stronger than for the LCP. This is due to the RCP uplink transmitted from DSS-43, a 70-m antenna in Canberra, AU, while the LCP uplink is from DSS-34, a 34-m antenna also in Canberra, AU. Both stations transmitted at 20 kW transmitter power.

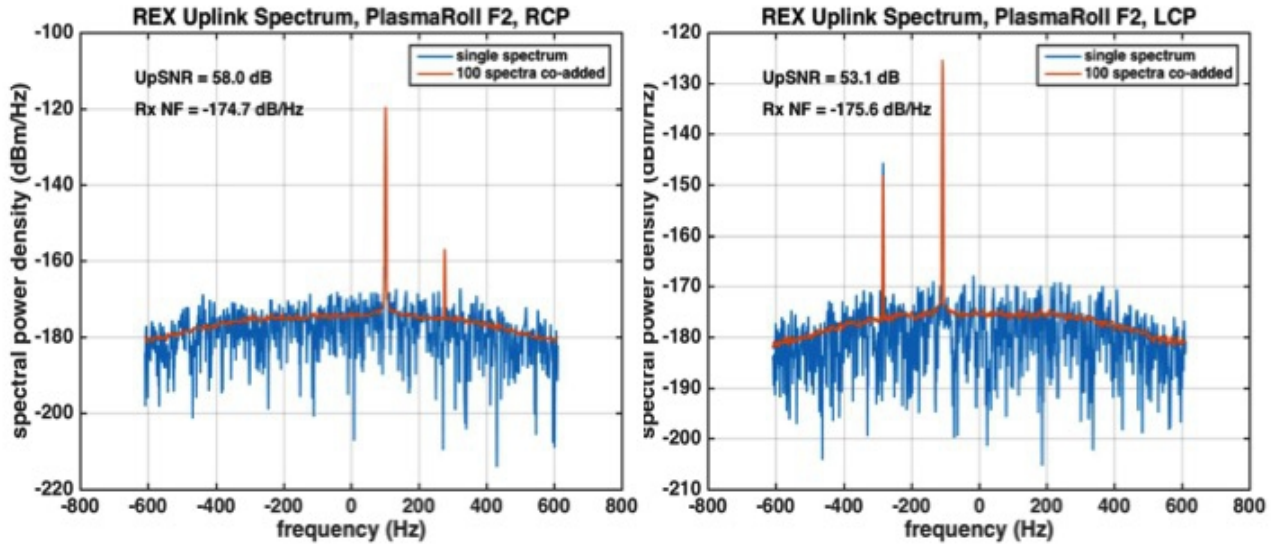


Figure 3.7.1. REX Uplink Spectra from PlasmaRoll F2. The PlasmaRolls were spacecraft measurements designed primarily for detecting the solar wind in situ by rolling the spacecraft along an Earth-pointed axis. Uplinks were transmitted and received on the spacecraft during the spacecraft roll. Using a link analysis the uplink's power is used to determine the peak of the uplink spectral line, and the power spectral density of the X-band receiver's noise floor is then scaled by the uplink to noise floor SNR.

The link analysis of the uplink's power registers the peak of the uplink spectral line in dBm. This registration is determined by integrating the power spectral density (psd), of the uplink under the spectral line. The spectrum of the uplink was computed using the FFT of the 1250-samples REX I's and Q's, windowed by a Hamming-type window (e.g. a Parzen window) in which the spectral width of the uplink signal is ~ 5 FFT bins wide. The integral of the uplink's spectral samples is scaled to the uplink power from the link analysis. The shape of the impulse response of the window, is fit to the spectral samples, and the shape's peak is the registration value. The psd of the X-band receiver's noise floor is scaled from the uplink's registration by the signal-to-noise ratio (SNR) from the spectral peak to the noise floor near baseband center. The 1.25 kHz bandwidth of REX's baseband channel is tapered toward band edge to suppress aliasing.

The psd of the X-band receiver's noise expected in the REX baseband spectra is,

$$P_N = k T_{XB} B$$

Where k is Boltzmann's constant, T_{XB} is the noise temperature of the X-band receiver's polarization channel and B is the channel's bandwidth. For $B = 1$ Hz, and the receiver noise temperatures from Table 3.2b.1, 149.6 K for RCP, and 138.8 K for LCP, the psd's are,

$$S_{XB}(RCP) = -176.85 \text{ dBm/Hz}$$

$$S_{XB}(LCP) = -177.17 \text{ dBm/Hz}$$

The noise floor psd values in Figure 3.7.1, are -174.7 dBm/Hz, and -175.6 dBm/Hz, respectively, are 2.1 dB and 1.5 dB larger respectively than expected. This discrepancy could come from the assumption in the link analysis that the uplink power was 20 kW, while the actual power transmitted by the station typically varies during the duration of the transmission. In addition, there is some uncertainty in the amount of RF power lost due to losses in cross polarization and RF switch efficiencies.

An additional recording by REX of uplinks occurred during the Pluto and Charon occultations, where four uplinks were transmitted by the DSN, two in RCP, and two in LCP. The spectrograms of these recordings are shown in Figure 3.7.2, where the two uplinks in each polarization are the strongest spectral lines. The two uplink signals from the cross polarization in each channel are the weaker cross-pol lines.

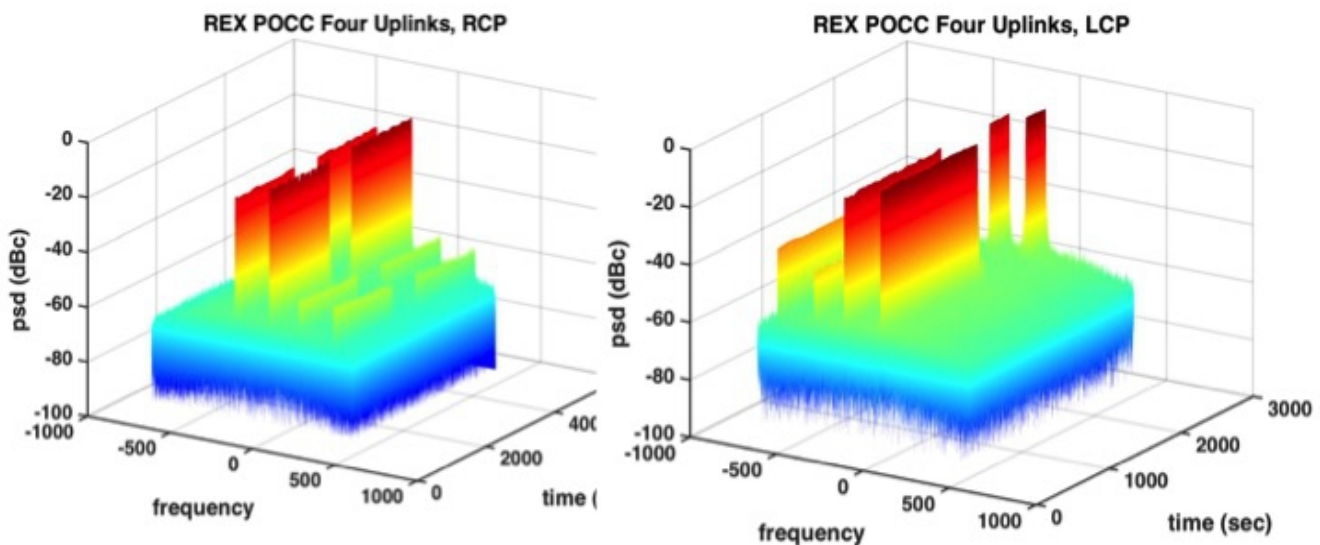


Figure 3.7.2. REX spectrograms of uplinks during the Pluto and Charon occultations. Four uplinks were transmitted to REX by the DSN, two in RCP, and two in LCP. The weaker spectral lines in the spectrograms are the cross-polarization signals.

Both polarizations of the REX recordings of the I and Q samples were low-pass filtered to isolate each of the four uplinks from each other. The complex representation $I + iQ$ samples were frequency shifted to 50 Hz from DC, and the I and Q sequences were separately digitally bandpass filtered in a 40 Hz band centered at 50 Hz. This separation was because the digital filter was a real-only process. The parallel I and Q filtered sequences were then recombined as $I + iQ$, into a complex representation. This process created two narrow band segments in the REX band, one containing just one of the uplinks, the other segment containing only the X-band receiver's noise. The power in the uplink is estimated from the segment containing the uplink and some of the receiver noise, and the spectral noise floor is estimated from the segment with only the noise, as can be seen in Figures 3.7.4, and 3.7.5. The SNR of the uplink is determined by summing the uplink's power spectral densities (psd) in the few spectral lines and subtracting the product of the noise floor psd multiplied by the number of bins used in the spectral line sum for the uplink power. Figure 3.7.4, and Figure 3.7.5, are the plots illustrating the result of the SNR's and psd's of the receiver noise.

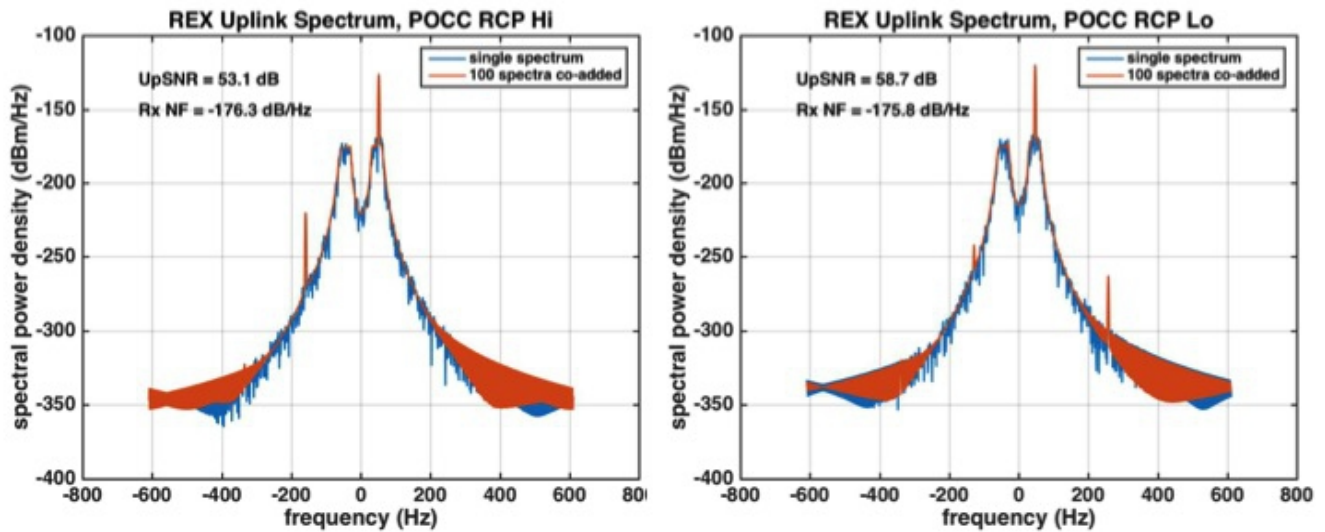


Figure 3.7.4. REX spectra of uplinks in RCP during Pluto and Charon Occultations. The two uplinks in each polarization have been isolated using a combination of frequency shifting and bandpass filtering. The portion of the spectrum containing the uplink signal is the 40 Hz section centered at +50 Hz, while the portion containing only the background noise is the 40 Hz section centered at -50 Hz. The uplink signals not selected are strongly rejected on the side lobe of the filter.

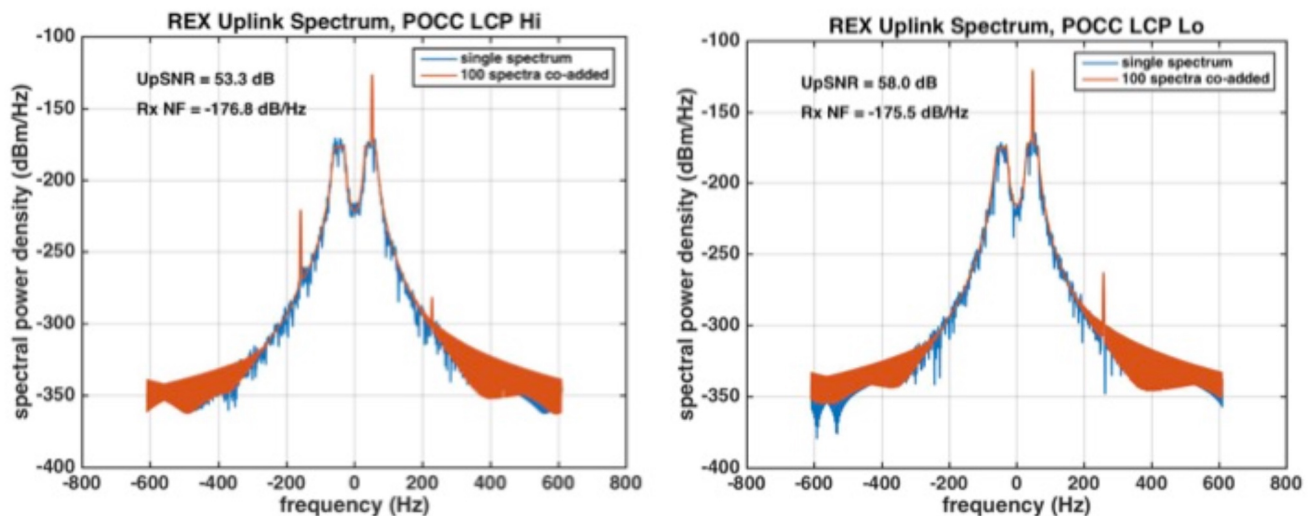


Figure 3.7.5. REX spectra of uplinks in LCP during Pluto and Charon Occultations. The two uplinks in each polarization have been isolated using a combination of frequency shifting and bandpass filtering. Identical to Figure 3.7.4, the portion of the spectrum containing the uplink signal is the 40 Hz section centered at +50 Hz, while the portion containing only the background noise is the 40 Hz section centered at -50 Hz. The uplink signals not selected are strongly rejected on the side lobe of the filter.

The power radiated by the DSN stations was logged for the Pluto and Charon occultations and used in the link analysis for an accurate estimate of the uplink power at REX. The registration and scaling of the power spectral density using this more accurate uplink power estimate improves the agreement between the resultant and expected receiver noise psd's. The agreement is within a few tenths of a dB.

The residual uncertainties likely reside in the losses the heterodyne process incurs converting the RF in the X-band antenna and feed down to the Radiometrics Channel's band and then to REX.

4.0 Conversion of REX units to Physical Units

The constants in Table 3.2b.1, converts REX units to the radiometric power in the REX channel in units of kelvins. Using Boltzmann's constant the temperature in Kelvin can be related to the total received power in the radiometrics channel in watts, P_{tot} :

$$P_{tot}(W) = kBT \quad (4.0.1)$$

where, k = Boltzmann's constant = 1.3807×10^{-23} J/K
 B = predetection bandwidth = 4.5 MHz
 $T (K) = T_{RX} + T_{ant}$

with, T_{RX} = system temperature (e.g. see Eqns 3.3.1, and 3.4.2)
 T_{ant} = antenna temperature (e.g. $T_{cold_sky}/2$ in Eqn 3.3.1)

For example, to convert REX units to power in dBm, with:

dBm : Decibels relative to 1 mWatt
 $dBm = 10 \cdot \log_{10}(\text{Power} \cdot 1000)$, (Power in watts)

A logarithmic form of Eqn 3.3.1 is useful:

$$\log_{10}(kT_{XB} P) = \log_{10} \left(k \frac{P_{REX \text{ units } P}}{G_P} \right) \quad (4.0.2)$$

The bandwidth B , has been removed in Eqn 4.0.2, with the understanding the power is now represented as a power spectral density, where for example the power in dBm, is now a power density, in units of dBm/Hz. The label P , denotes the two polarization channels, RCP and LCP. And is $P_{REX \text{ units } P}$, is the radiometric power in the REX channel, in REX units. Note, the bandwidth B , of the radiometrics channel has been incorporated into the receiver's gain, G_P . The gain setting of the receiver is G_{AGC} , and G_0 , is the gain word reference. Boltzmann's constant is incorporated in R_0 . The radiometric power in dBm, P_{dBm} , is the logarithmic expansion of Eqn 4.0.2, as:

$$P_{dBm} = R_G + 10 \log_{10}(RU) + g_{Step} (G_{AGC} - G_0) + R_0 \quad (4.0.3)$$

where, P_{dBm} , is the radiometrics total power in dBm
 R_G , is the radiometrics channel power due to receiver noise alone
 RU , are the REX units of the samples
 g_{Step} , is the receiver's gain step (equal to 0.475 dB)
 G_{AGC} , is the gain setting, also called the *gain word*
 G_0 , is the reference gain words, (fixed at RCP=167 and LCP=163, for Pluto)
 R_0 , is the REX units to Kelvin calibration constant incorporating Boltzmann's constant

Please be advised: The ten values of REX radiometric power, in REX Units ($RU_1, RU_2, \dots, RU_{10}$), presented in each REX FITS file (or REX frame), are sampled from an accumulating sum in the REX processor on the spacecraft. The cadence and alignment of these samples are discussed in Section 2.1, and again in Section 4.1 below. Importantly, the accumulator is cleared at the beginning of each REX frame, but immediately *after* the previous frame's total is captured. Hence, the first radiometer value in the REX frame, RU_1 , is the total integrated radiometer power of the previous frame.

Note: Eqn 4.0.3, is structured to have R_G , the power from receiver noise alone, as the base or reference to which power external to the receiver contributes. This choice however has the intrinsic redundancy that the receiver's noise power is also contained in the REX units, RU , and thus must be compensated in the scaling term R_θ .⁽¹⁾ Note as well, R_θ is calculated in the next section as the negative sum of the logarithms of the system temperature and the scaling factors for the respective polarizations.

The conversion of REX data to physical units, such as dBm, takes into account the bandwidth of the REX data. Because there are two REX data streams, associated with two REX bandwidths, (a) the 1.024 kHz, high data rate, narrowband channel, and (b) the 4.5 MHz low data rate, broadband radiometric channel, examples of conversion for both bandwidths will be illustrated here.

4.1 Conversion to dBm in the REX Broadband Channel

The REX data associated with the radiometric power in the 4.5 MHz bandwidth radiometrics channel for each polarization. The REX radiometric power is computed from digital samples of the RF voltage in the radiometrics channels.

By choosing the first radiometric value in REX each frame, the cadence of the radiometer power in the REX output data is once per REX frame.

The RF voltage samples are squared and accumulated in the REX processor. The value of the accumulator is reported in the REX output ten times per REX frame, and the accumulator is cleared after the tenth value is reported. The REX frames occur at a cadence of one frame every 1.024 seconds. Due to the idiosyncrasy of the REX processor, the last value of the accumulator, before the accumulator is cleared, is reported to the REX output as the first radiometric sample in the following frame.

The radiometric power in REX always has a contribution from the noise in the receiver. In addition, the radiometric power from the background sky may be present as well as the radiometric power from a radio source. The noise power of the receivers alone contributes an equivalent power in dBm/Hz:

$$P_{XB_RX_RCP_noise_only} = 10 * \log_{10}(k_{Boltzmann} T_{XB_RCP}) + 30 \text{ (dBm/Hz)}$$

$$P_{XB_RX_LCP_noise_only} = 10 * \log_{10}(k_{Boltzmann} T_{XB_LCP}) + 30 \text{ (dBm/Hz)}$$

(1) Some may find this redundancy unattractive, some do not. The author finds the distinction may fall along the lines of the perspective of a physicist or an engineer. The former values physical insight and intuition and the latter puts priority on order and efficiency. In any case, the choice does not affect the result of the conversion process from REX units to dBm.

Using the receiver noise temperatures from Table 3.2b.1,

$$P_{XB_RX_RCP_noise_only} = -176.852 \text{ dBm/Hz, RCP Rx noise only} \quad (4.1.1a)$$

$$P_{XB_RX_LCP_noise_only} = -177.177 \text{ dBm/Hz, LCP Rx noise only} \quad (4.1.1b)$$

The values in Eqn 4.1.1a, and 4.1.1b, are the values used for R_G in Eqn 4.0.3.

$$R_{G_RCP} = -176.852 \text{ dBm/Hz} \quad (4.1.1c)$$

$$R_{G_LCP} = -177.177 \text{ dBm/Hz} \quad (4.1.1d)$$

Equating Eqns 4.0.2 and 4.0.3, establishes the relationship between R_θ and R_G , as:

$$R_\theta = 10 \log_{10} \frac{k_{Boltzmann}}{G_{Pol}} - R_G + 30 \quad (4.1.2)$$

Using G_{REXtoK} for RCP and LCP from Table 3.2b.1, and R_G from Eqns 4.1.1a and 4.1.1b, above, Eqn 4.1.2 produces:

$$R_{\theta_RCP} = -101.030 \quad (4.1.3)$$

$$R_{\theta_LCP} = -104.547$$

Note: Those who would prefer to not have R_G redundant in the power conversion formula, can easily remove R_G from Eqn 4.0.3, and add R_G to Eqn 4.1.2.

As an example for REX looking at cold sky, the power in REX increases by one half the temperature equivalent of the cosmic microwave background, i.e. $T_{CMB}/2$, and the corresponding power in the REX channels becomes,

$$P_{XB_RX_RCP_noise+CMB/2} = -176.812 \text{ dBm/Hz, Rx noise plus CMB/2} \quad (4.1.4a)$$

$$P_{XB_RX_LCP_noise+CMB/2} = -177.134 \text{ dBm/Hz, Rx noise plus CMB/2} \quad (4.1.4b)$$

As a second example for the broadband REX radiometric samples from Cold Sky A observations as shown particularly in Figure 3.3.2, and starting with MET's of 330648120 for RCP, and 0330648134 for LCP, the REX RU's have mean values of,

$$RU_{coldskyA_RCP} = 1.285 \times 10^{10} \quad (4.1.5a)$$

$$RU_{coldskyA_LCP} = 2.882 \times 10^{10} \quad (4.1.5b)$$

and are consistent with the values in Table 3.3.1.

The application of Eqn 4.0.3, to the REX broadband data in Eqns 4.1.5a and 4.1.5b is:

$$dBm_{RCP} = -176.852 + 10 \log_{10}(RU_{BB_RCP}) - 0.475 (G_{AGC_RCP} - 167) + R_{\theta_RCP}$$

and for LCP:

$$dBm_{LCP} = -177.177 + 10\log_{10}(RU_{BB_LCP}) - 0.475 (G_{AGC_LCP} - 163) - R_{0_LCP}$$

The gain setting for the Cold Sky A data were 167, and 163 respectively, thereby removing the gain-dependent term. The scaling constants in Eqn 4.0.3, are $R_{0_RCP} = -101.030$, and $R_{0_LCP} = -104.547$, and with $G_{REXtoKelvin}$ from Table 3.2b.1, the radiometric power per Hertz is,

$$dBm_{RCP} = -176.794 \text{ dBm/Hz} \quad (4.1.6a)$$

$$dBm_{LCP} = -177.128 \text{ dBm/Hz} \quad (4.1.6b)$$

in agreement with Eqns 4.1.4a, and 4.1.4b, discrepancies of 0.02 dB and 0.01 dB.

4.2 Conversion to dBm in the REX Narrowband Channel

Both the bandwidth and the data format in the narrowband channel differ from the broadband channel. For completeness here is an example to illustrate the process of converting the REX narrowband data to dBm.

The REX narrowband data are I/Q (i.e. complex) samples from a low-pass filter with a 1.024 kHz bandwidth, and they are scaled voltages. The radiometric power in those samples is the complex-square of the samples, (i.e. $re^2 + im^2$). Using the narrowband REX data from the same Cold Sky A observations in Section 4.1, the Cold Sky A samples have mean values of,

$$RU_{coldskyA_RCP} = 1694.3 \quad (4.2.1a)$$

$$RU_{coldskyA_LCP} = 3857.9 \quad (4.2.1b)$$

These samples represent the power in the 1.024 kHz bandwidth of the narrowband channel. Presumably, they are larger by a factor of 1024, than the mean power of samples in a 1 Hz bandwidth, and smaller by a factor of $R_{NB2BB} = 1024/4.5 \times 10^6$, than the mean power of the samples in the broadband channel. However, the REX narrowband lowpass filters have their own gains, and additional factors of 1726 for RCP and 1700 for LPC, are needed to make the narrowband powers per Hertz equivalent to the broadband powers per Hertz. The application of Eqn 4.1, to the REX narrowband data, includes the scaling factor, $R'_{NB2BB} = R_{NB2BB}/1726$ (or 1700 for LPC).

For RCP narrowband:

$$dBm_{RCP} = -176.852 + 10\log_{10}(RU_{NB_RCP}/R'_{NB2BB}) - 0.475 (G_{AGC_RCP} - 167) + R_{0_RCP}$$

and for LCP narrowband:

$$dBm_{LCP} = -177.177 + 10\log_{10}(RU_{NB_LCP}/R'_{NB2BB}) - 0.475 (G_{AGC_LCP} - 163) - R_{0_LCP}$$

The gain setting for the Cold Sky A data were 167, and 163 respectively, removing the gain-dependent term. With the same scaling constants as in Section 4.1, $R_{0_RCP} = -101.030$, and $R_{0_LCP} = -104.547$, the radiometric power per Hertz is,

$$\text{dBm}_{RCP} = -176.797 \text{ dBm/Hz}$$

$$\text{dBm}_{LCP} = -177.131 \text{ dBm/Hz}$$

again in close agreement with Eqns 4.1.2a, and 4.1.2b.

Note that not all REX radiometer data, if converted to physical units will produce physically reasonable values since not all REX Radiometer data was taken with an external radiometric source in the beam of the HGA. For example, a typical REX measurement consists of first switching REX to an internal set of test patterns where REX produces data that can be bit-by-bit compared to the expected response. The REX Radiometer power will not be physically reasonable for any of the test pattern data.

5.0 Summary

Through the use of calibration targets with known radiometric brightness temperatures or flux, the REX Radiometer was calibrated using a multi-dimensional optimization to find the conversion constant and receiver noise temperature for the RCP and LCP channels. The optimizer used an L2 norm, defined in Eqn. 3.1.1, to find the optimum values of the conversion constants and the receiver noise temperatures. These results were the starting values for an equalization algorithm, detailed in Figure 3.2b.2, that produced calibrators and radiometric brightness temperature profiles consistent with no circular polarization. The values of these calibration constants are listed here in Table 5.1.

	REX units to Kelvin (10^6 to K)	Rx Noise Temperature (K)
RCP	84.76 ± 0.1	149.6 ± 0.1
LCP	205.26 ± 0.1	138.8 ± 0.1

Table 5.1. REX Radiometer Calibration Constants. The uncertainties are statistical, the consequence of propagating the standard deviations of the radiometric power measurements through the optimization and equalization algorithms.

The calibration for REX and the conversion from REX units radiometric power is contained in the constants, R_{G_RCP} , R_{G_LCP} , R_{0_RCP} , R_{0_LCP} , g_{step} , G_{AGC} and G_0 . But for the latter portion of the New Horizons Mission, and particularly for the Pluto Encounter, G_{AGC} equaled G_0 , and the REX calibration is contained solely in, R_{0_RCP} , R_{0_LCP} , the values for which are based on the conversion constants listed in Table 5.1, and include the four scaling constants,

$$R_{G_RCP} = -176.852 \text{ dBm/Hz}, \text{ and } R_{G_LCP} = -177.177 \text{ dBm/Hz}$$

$$R_{0_RCP} = -101.030, \text{ and } R_{0_LCP} = -104.547.$$

6.0 References

Benz, A.O., Radio emission of the quiet Sun, in: Landolt-Börnstein New Series VI/4B, Springer, (2009).

Condon, J.J., Cotton, W.D., Greisen, E.W., Yin, Q.F., Perley, A, Taylor, G.B., and Broderick, J.J., “The NRAO VLA Sky Survey,” *Astron J.*, 115,1693-1716, May(1998).

Deboy, C., Fountain, G., Funk, L, Haskins C., Hersman, C., Linscott, I., Mallder, V., Nguyen, H., and Vincent, M., “New Horizons RF REX Technical Reference Document,” The Johns Hopkins Applied Physics Laboratory Report 7399-9371(2007).

Deboy, C., and Funk, L, “New Horizons Telecommunication Subsystem to REX ICD,” The Johns Hopkins Applied Physics Laboratory Report 7399-9202, (2003).

Efimov, A.I., L.N. Samoznaev, M.K. Bird, I.V. Chashei, D. Plettemeier, “Solar wind turbulence during the solar cycle deduced from Galileo coronal radio-sounding experiments,” *Advances in Space Research*, 42 (2008) 117-123.

HEASARC Archive, RADIO – Master Radio Catalog,
<https://heasarc.gsfc.nasa.gov/W3Browse/all/radio.html>

Ho, C., S. Slobin, A. Kantak, S. Asmar, Solar brightness temperature and corresponding antenna noise temperature at microwave frequencies, IPN Progress Report 42-175, (2008).

Perley, R.A., Dreher, J.W., and Cowan, J.J., “The jet and filaments in Cygnus A,” *Astrophys. J.*, part 2, Letters to the Editor (ISSN 0004-637X), vol. 285, Oct. 1, p. L35-L38, (1984).

Rebold, T.A, Peng, T.K., and Slobin, S.D., “X Band Noise Temperature Near the Sun at a 34-m high Efficiency Antenna,” TDA Progress Report, 42-93 (1988)

Schulze, R., “Calculated Performance of the New Horizon High Gain Antenna System,” The Johns Hopkins Applied Physics Laboratory, Report SER-05-074, (2005).

Schulze, R., and Deboy C. private communication, (2017).

Seban, R., Ida Baker, Ivan Linscott, Kamal Oudrhiri, and Michael Vincent. "Preparing and Implementing the New Horizons Uplink Occultations: Applying Concepts, Tools, and Lessons Learned Over Nearly a Decade of Flight to Achieve a Successful Operation", SpaceOps 2016 Conference, SpaceOps Conferences, (AIAA 2016-2537)

Stern, A., et. al., “The Pluto System, Initial Results from Its Exploration by New Horizons,” *Science*, v360, 10.1126, Oct. (2015).

Tyler, G. L., I.R. Linscott, M.K. Bird, D.P. Hinson, D.F. Strobel, M. Pätzold, M.E. Summers, K. Sivaramakrishnan, “The New Horizons Radio Science Experiment (REX),” *Space Science Reviews*, Volume 140, Nos 1–4, 217–259, (2008).

Vinyaikin, N., “Frequency Dependence of the Evolution of the Radio Emission of the Supernova Remnant Cas A,” *Astronomy Reports*, Vol. 58, No. 9, pp. 626–639, (2014).

Wielebinski, R., “A History of Radio Astronomy Polarization Measurements,” *J. Astronomical History and Heritage*, 15(2), 76-95 (2012).

Zirin, H., B.M. Baumert, G.J. Hurford, The microwave brightness temperature spectrum of the quiet Sun, *Astrophys. J.* **370**, 779-783, (1991).